05

Superplasticity of ultrafine-grained Al−Mg−Sc−Zr alloys with different Mg, Sc, Zr content

© V.N. Chuvil'deev, M.Yu. Gryaznov, S.V. Shotin, A.V. Nokhrin, K.V. Likhnitskii, Ya.S. Shadrina, M.K. Chegurov, V.I. Kopylov, A.A. Bobrov

Lobachevsky University of Nizhny Novgorod,
603022 Nizhny Novgorod, Russia
e-mail: nokhrin@nifti.unn.ru

Received November 20, 2024
Revised May 16, 2025
Accepted July 8, 2025

Effect of magnesium concentration (2.5, 4.0, 6.0 wt.%) on the superplasticity of Al−Mg−Sc−Zr aluminum alloys with different Sc/Zr ratios (Sc/Zr = 0.45, 1.0, 2.2) has been studied. The ultrafine-grained (UFG) alloys are obtained by the Equal-Channel Angular Pressing. Superplasticity tests were carried out in the temperature range from 300 °C to 500 °C and in the range of strain rates ($\dot{\varepsilon}$) from $3.3 \cdot 10^{-4}$ to $3.3 \cdot 10^{-1}\,s^{-1}$. The maximum elongation to failure (δ_{max}) is reached at $\dot{\varepsilon} = 3.3 \cdot 10^{-2}\,s^{-1}$. At a test temperature of 500 °C, the maximum elongation to failure is $\delta_{max} = 1970\,\%$ (alloy with 2.5 % Mg and Sc/Zr = 2.2) and $\delta_{max} = 1750\,\%$ (alloy with 2.5 % Mg and Sc/Zr = 1.0). When fine-grained alloys with a high zirconium content are heated, simultaneous homogeneous precipitation of $Al_3(Sc,Zr)$ particles and discontinuos precipitation of fan-shaped submicron Al_3Zr particles are observed. An increase in the Sc concentration leads to a decrease in the number of Al_3Zr particles formed by the discontinous mechanism and to an increase in the number of Al_3Sc nanoparticles. An increase in Mg concentration leads to a decrease in the flow stress and El of fine-grained Al−Mg−Sc−Zr alloys. Studies of the microstructure show that strain-induced grain growth develops with superplasticity. The nature of the elongation to failure dependence on the test temperature is determined by the Sc/Zr ratio — in alloys with Sc/Zr ≥ 1, an increase in temperature leads to an increase in ductility, and in alloys with Sc/Zr = 0.45, to a decrease in ductility.

Keywords: Al−Mg alloys, scandium, zirconium, superplasticity, grain growth.

DOI: 10.61011/TP.2025.12.62407.426-24

Introduction

The high-strength Al−6% Mg−Sc−Zr alloys are currently extensively used in the industry (the grades 01570, 01570C, 01575, etc.) and they have an optimal combination of strength and plasticity at the room temperature, weldability and fatigue strength [1,2]. (Hereinafter, concentrations of the alloying elements are indicated in wt.%.) The Al−6% Mg−Sc−Zr alloys with an ultra-fine grain (UFG) microstructure, which are obtained by severe plastic deformation (SPD), demonstrate high superplasticity characteristics (SP) at the elevated temperatures and strain rates [3–5].It allows superplastic punching of complex-shape products from these alloys.

Elongation to failure for the ultra-fine Al–Mg–Sc–Zr alloys is quite high and exceeds characteristics of almost all other aluminum alloys. The most studied are the UFG 1570 alloy of the composition Al–(5.3−6.3)% Mg–(0.2−0.6)% Mn–(0.17–0.27)% Sc–(0.05–0.15)% Zr as well as the UFG 1570C alloy of the composition Al–(5.0−5.6)% Mg–(0.2−0.5)% Mn–(0.18−0.26)% Sc–(0.05−0.12)% Zr.

In the 1570 alloy with an average grain size $d_0 \sim 1\,\mu m$, which is produced by Equal-Channel Angular Pressing (ECAP), elongation to failure can be up to $\delta_{max} \sim 2000\,\%$ (at the temperature of 450 °C and the strain rate $\dot{\varepsilon} = 5.6 \cdot 10^{-2}\,s^{-1}$) [6]. In the study [7], the following higher SP characteristics were obtained in the 1570 alloy also produced by ECAP: $\delta_{max} \sim 2330\,\%$ at 450 °C, $\dot{\varepsilon} = 1.4 \cdot 10^{-1}\,s^{-1}$. High values of elongation to failure in the 1570 alloy are also obtained when using High Pressure Torsion (HPT) ($\delta_{max} \sim 1460\,\%$ at 400 °C, $\dot{\varepsilon} = 1 \cdot 10^{-2}\,s^{-1}$) [8]. The superplastic characteristics of traditionally-rolled alloys are usually lower that the characteristics of the UFG alloys produced by SPD (see, for example, [9–12]). Presently, the highest superplastic characteristics are achieved in the UFG 1570 alloy when applying an asymmetrical rolling process (ASR) with subsequent annealing: $\delta_{max} \sim 3170\,\%$ at 500 °C, $\dot{\varepsilon} = 5 \cdot 10^{-2}\,s^{-1}$ [13,14].

In the 1570C alloy, the maximum superplastic characteristics are achieved when applying thermal ECAP: $\delta_{max} \sim 4100\,\%$ at 450 °C, $\dot{\varepsilon} = 5.6 \cdot 10^{-2}\,s^{-1}$ [3]; $\delta_{max} \sim 3300\,\%$ at 475 °C, $\dot{\varepsilon} = 5.6 \cdot 10^{-2}\,s^{-1}$ [15]. The quite high superplastic characteristics in the 1570C alloy are also obtained when applying Friction Stir Process (FSP) [16–19] and rolling [4,20]. We should mention the study [21], which has analyzed the effect of SPD on the superplastic properties of the 1570C alloy and showed that the effect of SPD is manifested via a change of the average grain size, variation in a grain size and a portion of large-angle grain boundaries. The maximum superplastic characteristics are

obtained in the 1570C alloy with a large volume portion of the large-angle grain boundaries ($\sim 97\,\%$) and the average grain size $d_0 \sim 3.3\,\mu$m.

We note that magnesium reduces intensity of grain-boundary diffusion processes in aluminum [22,23] and is often considered as an element that provides increased stability of the non-equilibrium UFG microstructure in the aluminum alloys [24]. Therefore, the increased Mg concentration provides high physical-chemical properties and operating characteristics of the alloys of the Al–Mg system [1,2,25]. At the same time, it should be noted that Mg solubility in aluminum in equilibrium conditions is not very high (~ 1.5–1.9 wt.% at 100 °C [26]), thereby resulting in precipitation of β-phase particles along grain boundaries/dendrite boundaries during crystallization or provoking annealing. (Hereinafter, the term „provoking annealing“ is understood as a kind of low-temperature thermal treatment, which facilitates precipitation of the β-phase particles along the aluminum grain boundaries and, as a result, leads to a sharp increase of an intercrystallite corrosion rate.) The formed β-phase particles create microgalvanic pairs „the Al grain — the grain-boundary β-phase“ and reduce resistance of the aluminum alloys to intercrystalline corrosion. We note that centers for secondary formation of the β-phase particles during annealing can be Al_3(Sc,Zr) particles, which provide increased strength of the aluminum alloys [27]. It contributes to additional reduction of corrosion resistance of the aluminum alloys.

The present study is aimed at investigating the effect of the Mg concentration on an SP behavior of the UFG Al–Mg–Sc–Zr alloys with various Sc/Zr ratios, wherein special attention in the study is paid to alloys with a reduced magnesium content and an increased zirconium content (with the low Sc/Zr ratio). Reduction of the magnesium concentration in the Al–Mg–Sc–Zr alloys will make it possible to provide their increased corrosion resistance — provided that their strength (hardness) and high SP characteristics are preserved. Varying the Sc/Zr ratio in the composition of the Al–Mg–Sc–Zr alloys can be used for solving a task of partial substitution of expensive scandium with cheaper Zr (see also [28–30]). We note that a high price of scandium limits prospects of application of the industrial the Al–Mg–Sc–Zr alloys in civil mechanical engineering and power engineering. Therefore, practically, it is important to reduce the concentration of expensive Sc in the composition of the Al–Mg–Sc–Zr alloys.

1. Experimental procedure

The research object is the Al–Mg–Sc–Zr alloys with the various content of Mg = 2.5 %, 4.0 % and 6.0 %. For each magnesium concentration, we studied the alloys with 0.22 % Sc + 0.10 % Zr (Sc/Zr = 2.2), 0.16 % Sc + 0.16 % Zr (Sc/Zr = 1.0) and 0.10 % Sc + 0.22 % Zr (Sc/Zr = 0.45). Results of the studies of the alloys with 6 % Mg were previously published [30], while results of the studies of the alloys with 2.5 % and 4 % Mg are published for the first time.

Blanks of the aluminum alloys of the size $20\times20\times160$ mm were produced by induction casting in vacuum using a caster Indutherm VTC 200V with a copper mould and a ceramic crucible. The following casting modes were used: a melting point of 800 °C, a component meltdown time was 6–10 min, a casting temperature of 760 °C, a pre-casting holding time of 60 min, the were cooled to the room temperature for 50–250 s. A deviation of the real concentration of Sc and Zr from the design one did not exceed $-2\cdot10^{-3}$ %. A spread of the Mg concentration in various portions of the samples was ±0.2 %.

The UFG microstructure in the alloys was formed by ECAP using a hydraulic press Ficep HF400L under the following mode: $N = 3$ cycles of pressing at the temperature of 275 °C at the speed of 0.4 mm/s, in a square-sectioned fixture with an channel intersection angle of 90°. The samples were annealed for 30 minutes in an air furnace EKPS-10. The annealing temperatures (300 °C–500 °C) corresponded to the SP test temperatures (see below). The annealing time (30 min) corresponded to an average SP time (including a time of sample heating to the test temperature and of 10-minute isothermal sample holding at this temperature prior to the test start to set thermal equilibrium). The structure and the properties of the annealed samples were studied to determine a mechanism of precipitation of the Al_3(Sc,Zr) second-phase particles that provide stability of the microstructure under the SP conditions and affect stability of a superplastic flow.

For the SP tests, we used „dumb-bell“ samples with a working part of the size $2\times2\times3$ mm. The total length of the samples was 25 mm. The tensile tests were performed using a universal testing machine Tinius Olsen H25K-S at the strain rates $3.3\cdot10^{-4}$, $3.3\cdot10^{-3}$, $3.3\cdot10^{-2}$ and $3.3\cdot10^{-1}\,s^{-1}$ (tensioning rates are 10^{-3}, 10^{-2}, 10^{-1} and 1 mm/s, respectively) within the temperature interval from 300 °C to 500 °C. Based on analysis of a dependence „engineering stress (σ) — engineering strain (ε)“ we determined a flow stress (σ_b) and relative elongation to failure ($\delta_{\max}$) for the samples. Determination of an error $\delta_{\max}$ included comparison of elongation to failure measured by the curve $\sigma(\varepsilon)$ with elongation of the working part of the sample before and after the SP tests.

The test results were analyzed using an equation

$$\dot{\varepsilon} = A(\sigma_b/G)^{1/m}(b/d)^p(D_{\text{eff}}/b^2)(G\Omega/kT). \qquad (1)$$

where m is a rate sensitivity coefficient, $p = 2, 3$ is a numerical coefficient, b is a Burgers vector, G is a shear modulus, k is the Boltzmann constant, $D_{\text{eff}} = D_0\exp(Q_{\text{eff}}/kT)$ is an effective diffusion constant, Q_{eff} is energy of activation of SP strain [31,32].

In order to determine the parameters of the equation (1), the dependences „engineering stress (σ) — engineering strain (ε)“ are recalculated into dependences „true stress

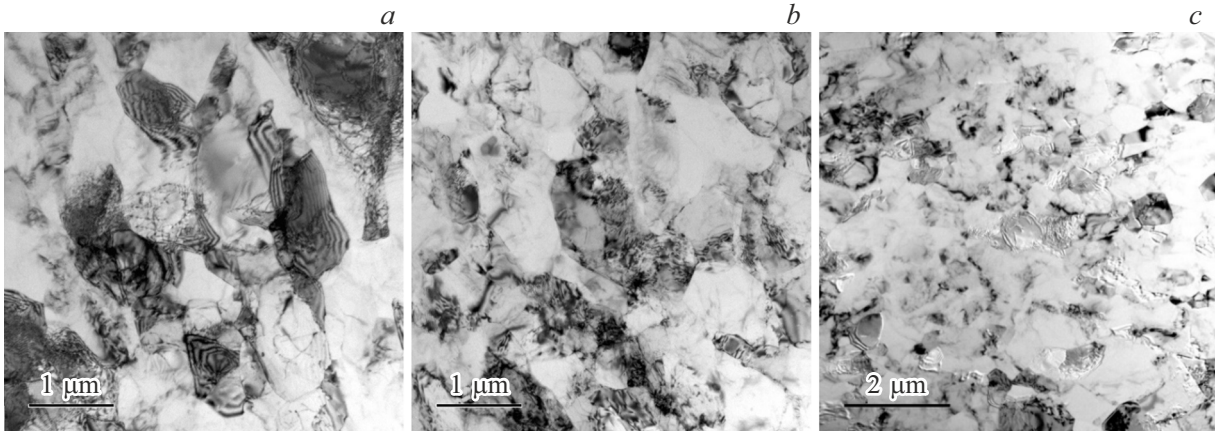

Figure 1. Microstructure of the UFG alloys with Sc/Zr = 2.2 and the various magnesium concentration: *a* — 2.5% Mg; *b* — 4% Mg; *c* — 6% Mg [30]. TEM.

(σ_t) — true strain (ε_t)„ according to the study [33]:

$$\varepsilon_t = \ln(1 + \varepsilon/100), \quad \sigma_t = \sigma(1 + \varepsilon_t). \qquad (2)$$

The microstructure of the alloys was studied using a metallographic microscope Leica DM IRM, a scanning-electron microscope (SEM) Jeol JSM-6490 and a transmission electron microscope (TEM) Jeol JEM-2100F. The samples for structure studies were mechanically ground and polished using diamond pastes of various dispersity and were finally polished using suspension based on aluminum oxide submicron powders and etched in a mixture of acids HF (15 ml), HNO_3 (10 ml) and glycerol (35 ml). The microstructure was metallographically studied in a collapse area (Zone I) and in an unstrained part of the samples (Zone II) after the SP tests. In order to detect shallow pores occurring as a result of etching the β-phase particles as well as well-oriented aluminum grains with the increased magnesium concentration, the metallographic studies were performed in a mode of interference contrast with two light filters (polarizational, lambda). In this mode the shallow pores were dyed in a green color, thereby making it possible to separate deep strain-origin pores occurring during superplastic strain and shallow corrosion-origin pores. The average size of grains and pores was calculated by a chord method using the GoodGrains software. The composition of the precipitating $Al_3(Sc,Zr)$ particles was analyzed using an X-ray microanalyzer included in the microscope Jeol JEM-2100F. The composition of the coarse β-phase particles was analyzed using an X-ray microanalyzer Oxford Instruments INCA 350 included in the microscope Jeol JSM-6490. Cleavages were fractographically analyzed by the SEM method.

2. Results

2.1. Microstructure studies

The UFG alloys with 2.5 % Mg in a post-ECAP state have a homogeneous microstructure with the average grain size $\sim 0.6-0.8\,\mu$m; the grains do not exhibit significant anisotropy. The increase of the Mg concentration from 2.5 % to 6% results in slight reduction of the average grain size to $\sim 0.3-0.5\,\mu$m (Fig. 1).

When the UFG Al–Mg–Sc–Zr alloys are heated, the $Al_3(Sc,Zr)$ particles precipitate (Fig. 2). When the UFG Al–6% Mg–Sc–Zr alloys with the increased scandium content are heated, the Al_3Sc particles are formed and they precipitate in a grain volume and along cores of lattice dislocations (Fig. 2, *a*). The alloys with the increased zirconium content exhibit formation of three types of the particles — within the grain volume the nanoparticles Al_3Sc and $Al_3(Sc_{0.5}Zr_{0.5})$ are formed and near the grain boundaries the fusiform submicron Al_3Zr particles precipitate by the discontinuous decomposition mechanism. These particles formed by the discontinuous decomposition mechanism are marked in Fig. 2, *b* by a yellow dashed line. The size and composition of the precipitating particles were investigated in detail in our previous study [30]. Results of energy-dispersive microanalysis of the composition of the secondary particles formed when annealing the alloy with Sc/Zr = 0.45 are shown in Fig. 3. Annealing the Al–6% Mg–0.16% Sc–0.16% Zr alloys exhibits single formation of the Al_3Zr particles by the discontinuous decomposition mechanism, but the number of the fusiform particles in the alloys with Sc/Zr = 1 is much less than in the alloys with Sc/Zr = 0.45. Reduction of the Mg concentration results in an increase of a volume portion of the $Al_3(Sc,Zr)$ particles, but does not affect a nature of their formation.

We note that discontinuous formation of the Al_3Zr particles when annealing the fine-grained aluminum alloys was previously described in the studies [34–38]. Although, it should be noted that causes of manifestation of the discontinuous decomposition in the Zr-enriched alloys are still understudied and quite often when annealing the UFG Al–Zr alloys the authors observe homogenous formation of the spherical Al_3Zr nanoparticles [39,40].

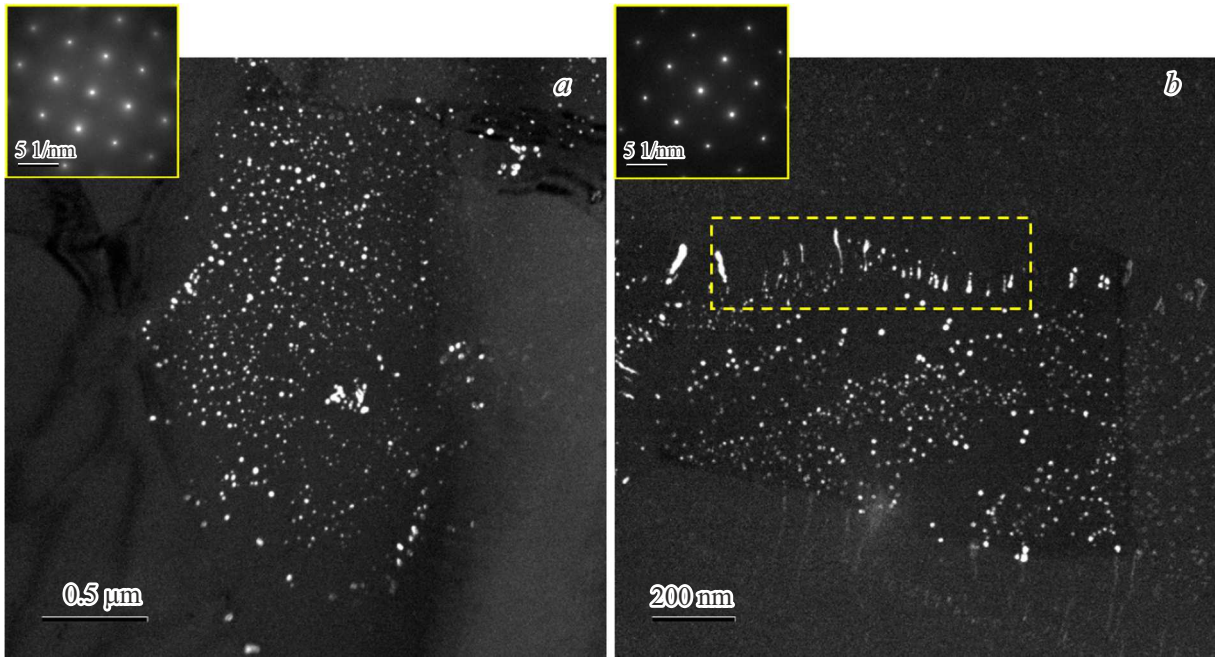

Figure 2. Al3(Sc,Zr) particles formed in the UFG alloys with 6% Mg and Sc/Zr = 2.2 (a) and Sc/Zr = 0.45 (b) after annealing at 500 °C, 30 min. TEM. Microdiffraction patterns were recorded from an area $\sim 10\,\mu m^2$ that included several grains.

Fig. 4 shows results of the studies of the microstructure of the annealed alloys with a various content of magnesium, scandium and zirconium. The precipitating $Al_3(Sc,Zr)$ particles provide stabilization of the non-equilibrium UFG microstructure of the Al−Mg−Sc−Zr alloys. The alloys with the increased zirconium content and the log magnesium content (2.5 %, 4 %) exhibit coarse recrystallized grains, whose size can be up to 10 μm (Fig. 4, b, d). The recrystallized microstructure in the annealed alloys with 6 % Mg has a high degree of homogeneity after heating to 500 °C (Fig. 4, e, f).

Fig. 4, g shows dependences of the average grain size on the temperature of 30-minute annealing of the UFG alloys with the different content of Mg, Sc, Zr. It is clear in Fig. 4, g that the temperature of start of grain growth is 350 °C−375 °C and weakly depends on the Mg concentration and the Sc/Zr ratio. The increase of the Mg concentration (when Sc/Zr = const) and the increase of the Sc/Zr ratio (when Mg = const) results in reduction of the average grain size. For example, in the alloys with Sc/Zr = 2.2 reduction of the Mg concentration from 2.5 % to 6 % results in reduction of the average size of the recrystallized grain from 4.3 to 2.1 μm (after annealing at 500 °C, 30 min). The similar increase of the Mg concentration in the alloys with Sc/Zr = 0.45 after annealing at 500 °C results in reduction of the grain size from 6.1 to 2.5 μm.

The recrystallized alloys exhibit traces of etching of the β-phase particles along the grain boundaries (Fig. 5). The alloys with the coarse grains exhibit larger pits of etching the β-phase particles, which are uniformly arranged over a section surface. The fine-grained alloys with a small grain size exhibit a large number of fine etching pits arranged along the grain boundaries (Fig. 5, a). The increase of the Mg concentration results in an increase of the number of the etching pits and a decrease of their size (due to reduction of the grain size in the alloys with the increase magnesium content).

2.2. SP tests of the fined-grained alloys

The results of the SP tests are generalize in Table 1 and in Fig. 6, a. It is clear in Fig. 6, a and in Table 1 that for the alloys with 0.22 % Sc + 0.10 % Zr and 0.16 % Sc + 0.16 % Zr the increase of the temperature of the test results in a monotonic increase of plasticity. The dependence of elongation to failure on the strain rate $\delta_{max}(\dot{\varepsilon})$ in these alloys is non-monotonic and maximum plasticity is achieved when $\dot{\varepsilon} = 3.3 \cdot 10^{-2}\,s^{-1}$ (Table 1). When $\dot{\varepsilon} = 3.3 \cdot 10^{-2}\,s^{-1}$ and the temperature is 500 °, the Al−2.5% Mg−0.22% Sc−0.10% Zr alloy exhibits plasticity $\delta_{max} = 1975\,\%$ (Fig. 6, b). Under similar temperature-rate conditions of strain, in the Al−2.5% Mg−0.16% Sc−0.1% Zr elongation to failure is $\delta_{max} = 1750\,\%$. At the lower strain temperatures, the value of elongation to failure of the alloys with the increased Sc content (Sc/Zr ≥ 1.0) decreases, but remains quite high (Table 1, Fig. 6, b). For example, in the Al−2.5% Mg−0.16% Sc−0.16% Zr alloy, when $T = 450$ °C and $\dot{\varepsilon} = 3.3 \cdot 10^{-2}\,s^{-1}$, relative elongation to failure can be up to $\delta_{max} = 1370\,\%$, while in the

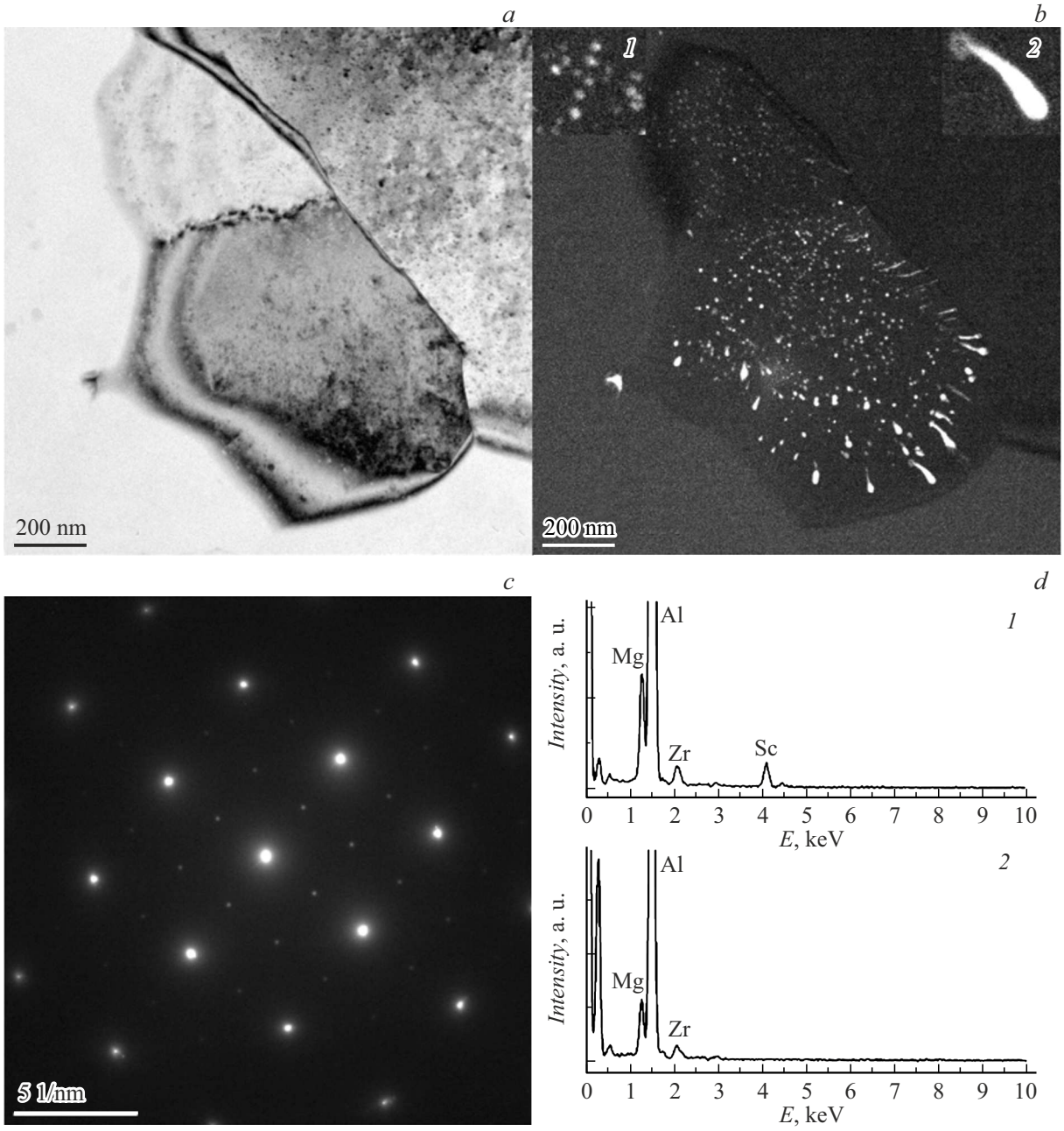

Figure 3. Results of the studies of the composition of the $Al_3(Sc,Zr)$ particles formed in the UFG Al–6Mg–0.10% Sc–0.22% Zr alloy after annealing at 500 °C, 30 min: *a* — a bright-field image of the studied grain *b* — a dark-field image of the particles in the studied grain: *1* — spherical nanoparticles formed in a homogenous decomposition mechanism; *2* — elongated particles formed by a discontinuous decomposition mechanism; *c* — a microdiffraction pattern of the analyzed grain of the area $\sim 1\,\mu m^2$, which is shown in *a,b*; *d* — X-ray (energy-dispersive) microanalysis of the composition of the particles №. 1 and №. 2 shown in *b*. TEM.

Al–2.5% Mg–0.22% Sc–0.10% Zr alloy, when $T = 400\,^\circ C$ and $\dot{\varepsilon} = 3.3 \cdot 10^{-2}\,s^{-1}$, it can be up to $\delta_{max} = 1140\,\%$.

In the fine-grained alloys with the increased zirconium content (Sc/Zr = 0.45) and the low magnesium content (2.5 %, 4 % Mg), the increase of the strain temperature results in reduction of plasticity (Fig. 6, *a*). It is a quite unexpected result, since it is traditionally assumed that the increase of the temperature results in an increase of plasticity of the fine-grained aluminum alloys [31]. In the fine-grained Al–6% Mg–0.10% Sc–0.22% Zr alloy, the increase of the temperature results in a slight increase of plasticity (when $\dot{\varepsilon} = \text{const}$).

Fig. 7, *a–d* shows the dependences $\sigma(\varepsilon)$ for the samples of the alloys with 2.5 (Fig. 7, *a, c*) and 4 % Mg (Fig. 7, *b, d*) at the temperatures of 400 °C (Fig. 7, *a, b*) and 500 °C (Fig. 7, *c, d*) (when $\dot{\varepsilon} = 3.3 \cdot 10^{-2}\,s^{-1}$). The curves $\sigma(\varepsilon)$ are typical for SP strain — a stage of fast strain hardening, which transits into a long loss-of-strength stage. The

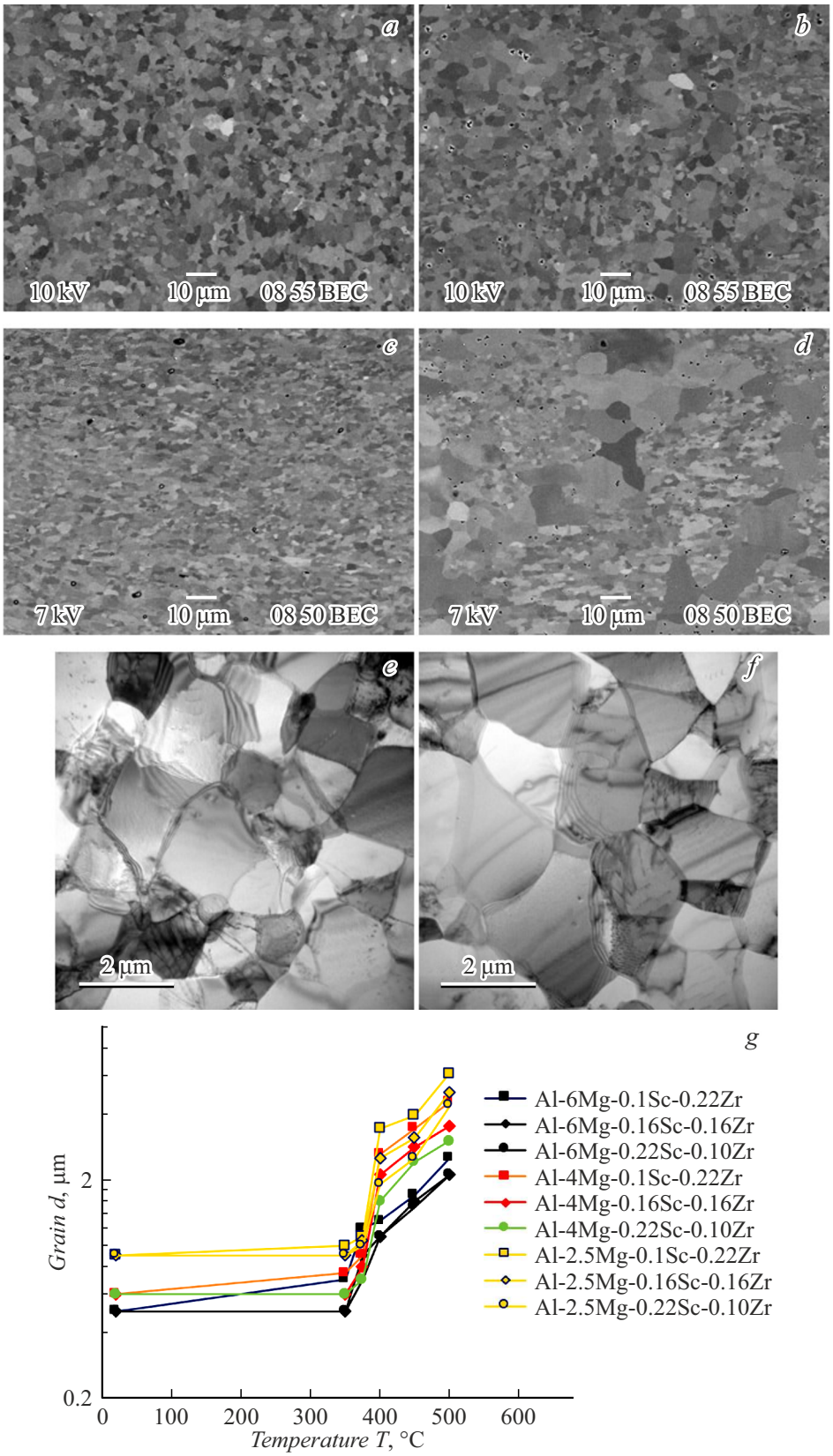

Figure 4. Effect of the annealing temperature on the microstructure of the UFG Al–Mg–Sc–Zr alloys. The microstructure of the alloys with 2.5 % (*a,b*), 4 % (*c,d*), 6 % Mg (*e,f*) and with Sc/Zr = 2.2 (*a,c,e*), Sc/Zr = 0.45 (*b,d,f*) after annealing at 500 °C, 30 min; *g* — the dependence of the grain size on the annealing temperature.

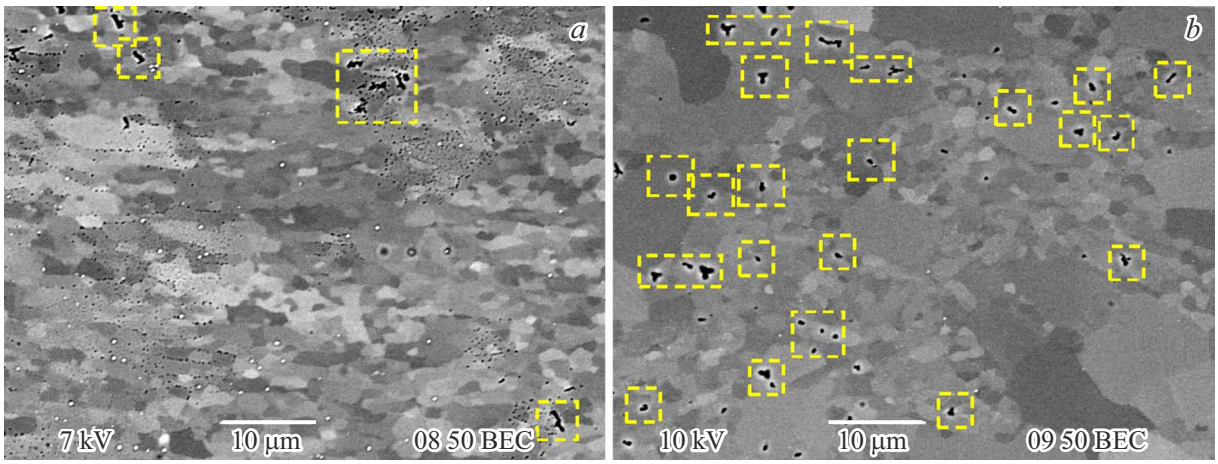

Figure 5. Microstructure of the Al–4% Mg–Sc–Zr alloys after annealing at 500 °C, 30 min: *a* — Sc/Zr = 2.2, *b* — Sc/Zr = 0.45. The largest pits of etching the β-phase particles are marked by a dashed line. SEM.

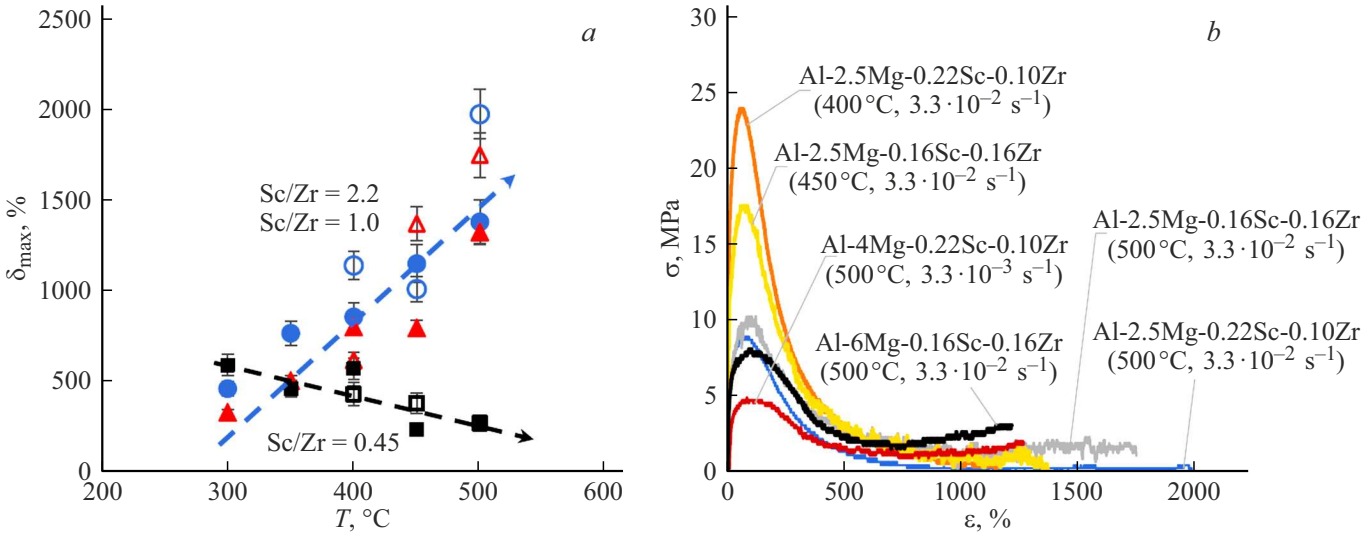

Figure 6. Results of the SP tests of the Al–Mg–Sc–Zr alloys: *a* — the dependences of elongation to failure on the temperature of tests of the alloys with 2.5 % Mg (the round markers — Sc/Zr = 2.2, the triangular markers — Sc/Zr = 1, the square markers — Sc/Zr = 0.45; the filled markers — $\dot{\varepsilon} = 3.3 \cdot 10^{-3}\,s^{-1}$, the unfilled markers — $\dot{\varepsilon} = 3.3 \cdot 10^{-2}\,s^{-1}$); *b* — the tensile curves of $\sigma(\varepsilon)$ of the alloys with maximum plasticity.

curves $\sigma(\varepsilon)$ for the alloys with 2.5 % Mg (Fig. 7, *a, c*) clearly exhibit stress surges that are related to a progress of dynamic recrystallization processes [4,5]. A value of the stress surge on the curves $\sigma(\varepsilon)$ for the alloys with 4 % Mg is much less than for the alloys with 2.5 % Mg (Fig. 7, *b, d*). The progress of the dynamic recrystallization processes with superplasticity of the Al–6% Mg–Sc–Zr alloys was previously described in the study [30].

At the temperatures 400 °C–500 °C and the high strain degrees ($\varepsilon > 700\,\%$–$800\,\%$), the curves $\sigma(\varepsilon)$ for the alloys with 4 % Mg exhibit a stress increase stage. At the high strain degrees, the similar stress increasing stage exhibits on the curves $\sigma(\varepsilon)$ for the UFG Al–6% Mg–Sc–Zr alloys (see [30]). According to the study [41], the increase of the flow stress is related to a strain-induced grain growth (see also the equation (1)).

Fig. 7, *e, f* shows dependences of relative elongation to failure and the flow stress on the Mg concentration in the fine-grained alloys. It is clear from the provided data that when $\dot{\varepsilon} = 3.3 \cdot 10^{-3}\,s^{-1}$ the increase of the Mg concentration results in a decrease of relative elongation to failure δ_{max} and, at the same time, a decrease of the flow stress σ_b. In particular, for the alloys with Sc/Zr = 2.2 at the temperature of 500 °C and the strain rate of $3.3 \cdot 10^{-3}\,s^{-1}$ the increase of the Mg concentration from 2.5 % to 6 % results in reduction of δ_{max} from 1380 % to 345 % and reduction of σ_b from 5.1 to 3.3 MPa. In the similar conditions of strain, the alloys with Sc/Zr = 1 exhibit reduction of δ_{max}

Table 1. Effect of the temperature and the strain rte on maximum elongation to failure (δ_{max}, %) of the fine-grained Al−Mg−Sc−Zr alloys with the different content of magnesium, scandium and zirconium

T, °C	$\dot{\varepsilon}$, s^{-1}	Al−2.5 % Mg			Al−4 % Mg			Al−6 % Mg [30]		
		Sc/Zr = 2.2	Sc/Zr = 1.0	Sc/Zr = 0.45	Sc/Zr = 2.2	Sc/Zr = 1.0	Sc/Zr = 0.45	Sc/Zr = 2.2	Sc/Zr = 1.0	Sc/Zr = 0.45
300	$3.3 \cdot 10^{-3}$	460 ± 40	330 ± 40	590 ± 30	530 ± 40	400 ± 30	800 ± 70	285 ± 20	325 ± 30	320 ± 30
350	$3.3 \cdot 10^{-3}$	765 ± 60	505 ± 50	460 ± 40	575 ± 50	675 ± 60	630 ± 60	–	785 ± 70	665 ± 60
400	$3.3 \cdot 10^{-4}$	–	–	–	365 ± 40	–	–	–	–	–
	$3.3 \cdot 10^{-3}$	855 ± 60	800 ± 60	570 ± 30	850 ± 70	610 ± 60	555 ± 50	710 ± 60	320 ± 30	350 ± 40
	$3.3 \cdot 10^{-2}$	1140 ± 70	615 ± 50	430 ± 40	530 ± 50	745 ± 50	380 ± 40	790 ± 50	905 ± 80	350 ± 40
	$3.3 \cdot 10^{-1}$	335 ± 40	300 ± 30	225 ± 30	–	–	275 ± 30	415 ± 40	425 ± 50	335 ± 40
450	$3.3 \cdot 10^{-3}$	1150 ± 60	795 ± 50	235 ± 20	–	–	–	895 ± 70	850 ± 60	795 ± 80
	$3.3 \cdot 10^{-2}$	1010 ± 60	1370 ± 70	380 ± 30	–	–	–	345 ± 40	295 ± 40	615 ± 60
	$3.3 \cdot 10^{-1}$	330 ± 20	345 ± 30	250 ± 30	–	–	–	165 ± 30	210 ± 30	405 ± 40
500	$3.3 \cdot 10^{-4}$	–	–	–	–	575 ± 40	–	–	–	–
	$3.3 \cdot 10^{-3}$	1380 ± 60	1325 ± 50	280 ± 30	910 ± 50	1265 ± 50	980 ± 60	345 ± 30	1005 ± 50	535 ± 40
	$3.3 \cdot 10^{-2}$	1975 ± 100	1750 ± 80	270 ± 20	1035 ± 50	1130 ± 60	395 ± 30	400 ± 50	1215 ± 60	705 ± 50
	$3.3 \cdot 10^{-1}$	505 ± 40	605 ± 40	275 ± 30	–	–	320 ± 40	860 ± 60	185 ± 20	390 ± 40

from 1320 % to 1005 % and reduction of σ_b from 5.8 to 3.4 MPa (Fig. 7, *e*). At the strain temperature of 500 °C, the magnesium effect on the superplastic characteristics of the Al−Mg−Sc−Zr alloys is similar, a scope of this effect is noticeably smaller (Fig. 7, *f*).

It is interesting to note that the effect of the Sc/Zr ration on plasticity of the Al−Mg−Sc−Zr alloys is different at the elevated ($T = 500$ °C) and decreased ($T \leq 400$ °C) temperatures of strain. At the temperature of 500 °C and the strain rate $\dot{\varepsilon} = 3.3 \cdot 10^{-3}\ s^{-1}$ maximum plasticity is observed for the alloys with Sc/Zr = 1 (Fig. 7, *e*), while at the temperature of 400 °C and below it is observed for the alloys with the increased scandium content (Sc/Zr = 2.2) (Fig. 7, *f*). The exception is a case of the SP tests at the temperature of 500 °C and the strain rate $\dot{\varepsilon} = 3.3 \cdot 10^{-2}\ s^{-1}$ — in these conditions plasticity of the Al−2.5% Mg−0.22% Sc−0.10% Zr alloy exceeds plasticity of the Al−2.5% Mg−0.16% Sc−0.16% Zr alloy, but a scope of this difference just slightly exceeds an error of determination of a value of δ_{max} (Table 1). The alloys with the increased zirconium content (Sc/Zr = 0.45) demonstrate lower plasticity with all the studied magnesium concentrations.

Fig. 8 shows SEM images of surfaces of cleavages of the samples of the fined-grained alloys after the SP tests. The cleavages of all the samples after the tests at the reduced temperatures were viscous and were a set of variously-sized pits. After the tests at $T = 500$ °C, the cleavages had a fine-cell microstructure, which indirectly indicates that failure occurred along the grain boundaries. The sample cleavages contain large pores, which indicate a cavitational nature of failure.

It should be noted that superplastic strain of the aluminum alloys with 2.5 % and 4 % Mg is accompanied with intense pore formation (Fig. 9). With the pre-defined Sc/Zr ratio and the constant Mg concentration, an increase of the strain degree results in an increase of a volume portion and a size of the pores. Results of the metallographic studies were analyzed to show that the increase of the scandium concentration resulted in reduction of susceptibility of the fined-grained alloys to pore formation. The alloys with the reduced magnesium content exhibit a minimum number of the pores. The pores are uniformly distribution along a strained part of the sample — their size and number decrease from the collapse area to the unstrained area according to distribution of strain in the sample. The metallographic studies show that the SP-formed pores are arranged mainly along the grain boundaries of the fine-grained alloys. The increase of the strain temperature results in an increase of the number and sizes of the pores in the strained part of the samples (Fig. 9, *a, b*).

The results of the metallographic studies show that a nature of evolution of the microstructure of the alloys is different at the elevated (500 °C) and decreased (below 450 °C) temperatures of strain. After strain at 500 °C the average grain size near the failure area is comparable with the grain size in the unstrained area (Fig. 10) and the grains keep their equiaxed size. This result indirectly indicates that a key SP mechanism under optimal temperature-rate conditions of strain is grain boundary sliding. It is

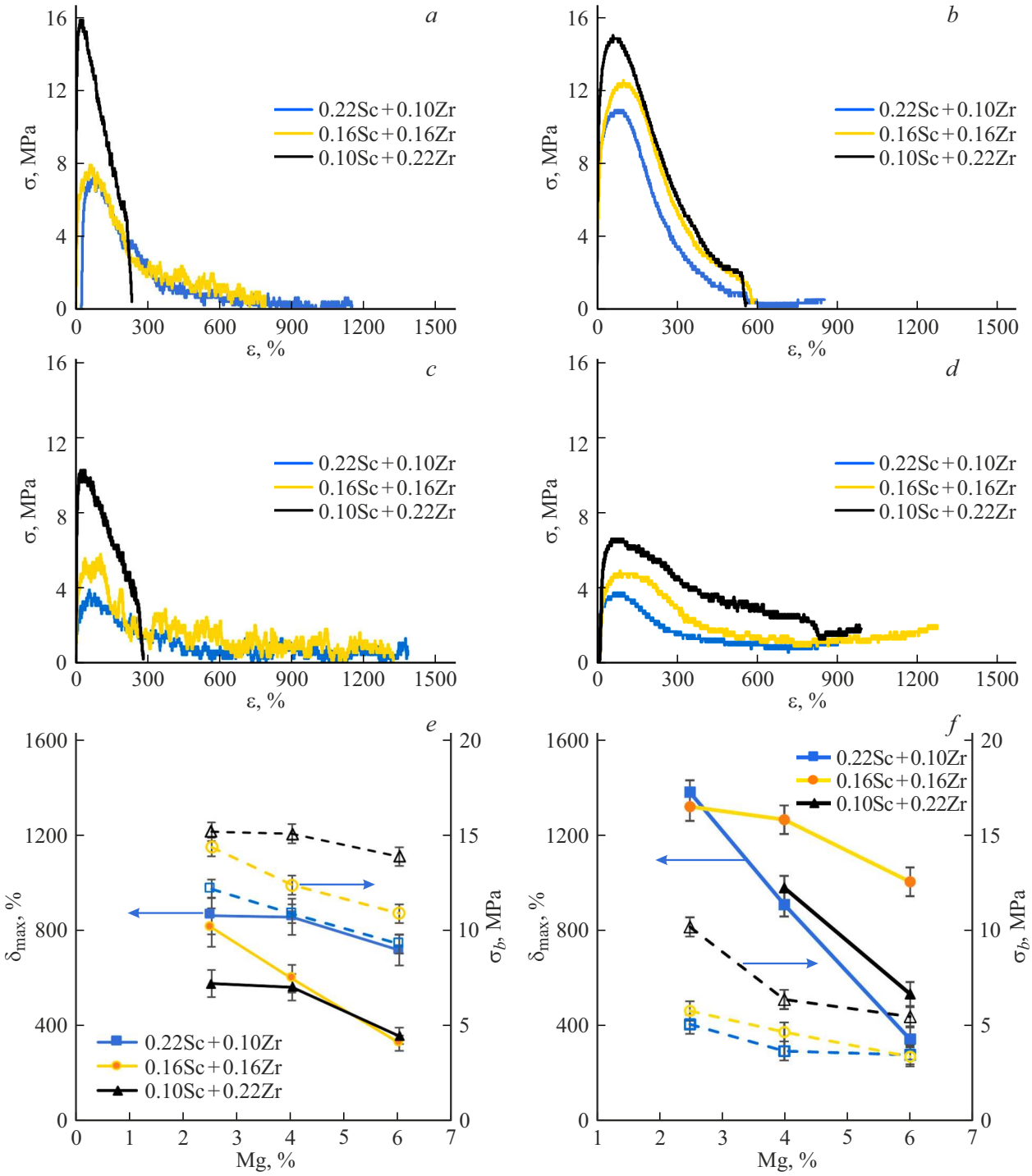

Figure 7. Tensile curves $\sigma(\varepsilon)$ of the alloys with 2.5 (*a,c*) and 4.0 % Mg (*b,d*); dependences of elongation to failure $\delta_{\max}$ (the solid lines) and the flow stress σ_b (the dashed liens) on the Mg concentration for the alloys with the different Sc/Zr ratio (*e,f*). The tests when $T = 400\,^{\circ}\mathrm{C}$ (*a,b*) and $500\,^{\circ}\mathrm{C}$ (*c,d*) and $\dot{\varepsilon} = 3.3 \cdot 10^{-3}\,\mathrm{s}^{-1}$.

important to not that the average grain size in the strained part of the samples after the SP tests at 350 °C–500 °C significantly exceeds the average grain size after annealing at the same temperature (Fig. 4,*g*, 10,*b*). It indicates that the SP process includes an intense strain-induced grain growth. At the increased strain rates, we observe grain elongation along a tensile-axis direction (Fig. 11), thereby indicating a significant contribution by intragranular sliding to sample elongation under conditions of high-rate strain. A green color in Fig. 10 and 11 belongs to shallow pores that are formed in a place of etching the β-phase particles and the aluminum grains, which have reduced resistance to impact by acids used for structure identification.

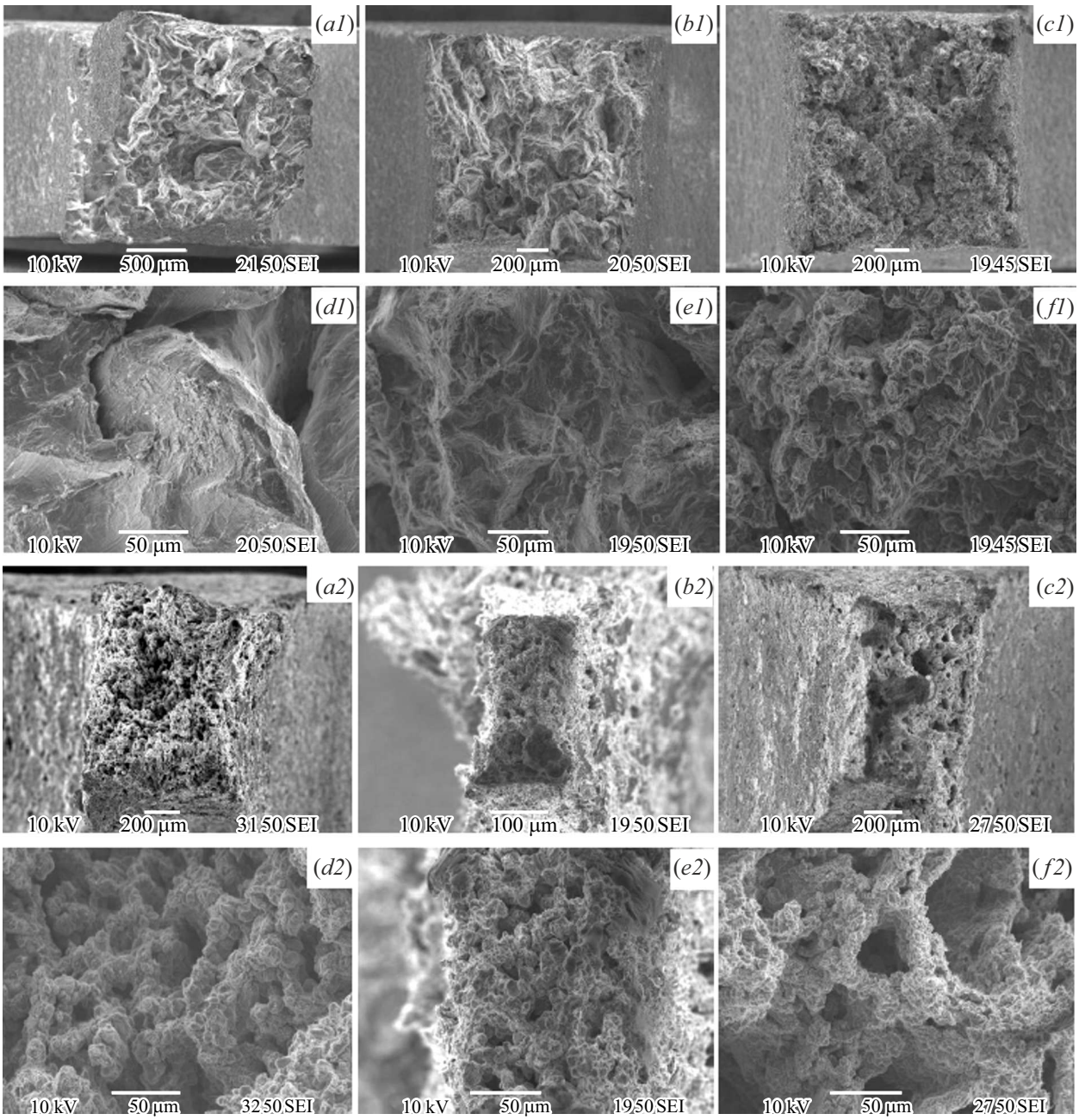

Figure 8. Fractographic analysis of cleavages of the samples of the fine-grained alloys with 4 % (*a1–f1*) and 6 % Mg (*a2–f2*) after the SP tests at the temperature of 500 °C and $\dot{\varepsilon} = 3.3 \cdot 10^{-3}\,\mathrm{s}^{-1}$: (*a1,d1,a2,d2*) Sc/Zr = 2.2, (*b1,e1,b2,e2*) Sc/Zr = 1; (*c1,f1,c2,f2*) Sc/Zr = 0.45. SEM.

The increase of the magnesium concentration results in reduction of the average grain size in the strained and unstrained parts of the samples. In the strained part of the samples (500 °C, $3.3 \cdot 10^{-3}\,\mathrm{s}^{-1}$) of the alloys with Sc/Zr = 2.2, reduction of the magnesium concentration from 6 % to 2.5 % results in an increase of the average grain size from 15–20 to 30–35 μm, and from 3.7 to 10–15 μm in the strained part of the samples of the alloys with Sc/Zr = 0.45. In the alloys with 2.5 % Mg and 4 % Mg, the effect of the Sc/Zr ratio on a nature of evolution of the microstructure is ambiguous — at the reduced temperatures (below 450 °C) the strained part of the samples of the alloys with the increased scandium content (Sc/Zr = 2.2) exhibits a smaller grain size, while at the temperature of 500 °C an unambiguous effect of the Sc/Zr ratio on the nature of evolution of the microstructure is not identified — the effect of the Sc/Zr ration turns out be less than an error of measurement of the grain sizes in the strained part of the samples of the alloys with 2.5 % Mg and 4 % Mg.

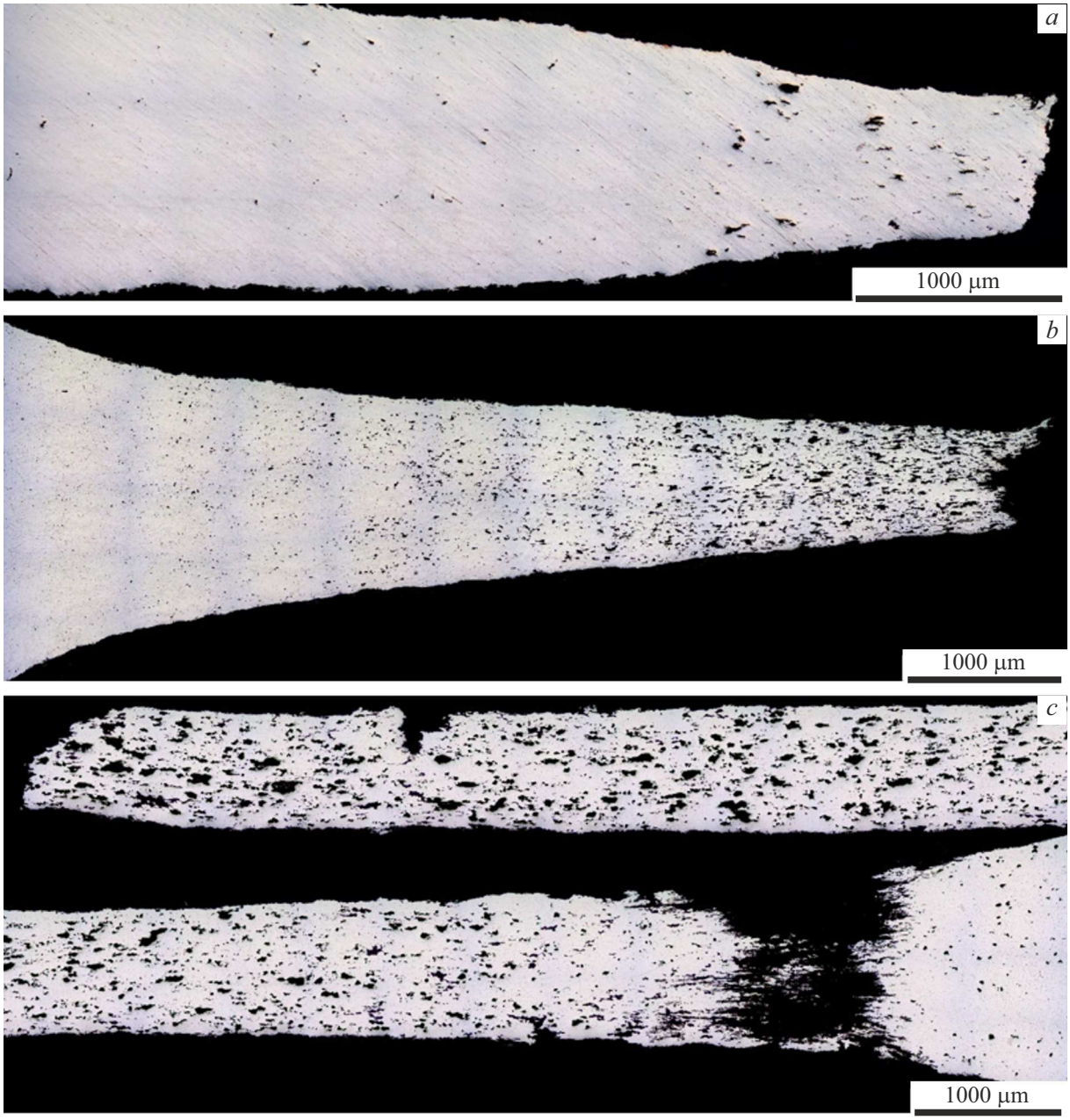

Figure 9. General view of the samples of the Al–4% Mg–0.22% Sc–0.10% Zr after the Sp tests at the temperatures of 300 °C (*a*), 400 °C (*b*) and 500 °C (*c*). $\dot{\varepsilon} = 3.3 \cdot 10^{-3}\,\mathrm{s}^{-1}$. Metallography.

3. Discussion of results

3.1. Analysis of the SP mechanisms

Let us analyze possible mechanisms of superplastic strain and mechanisms of failure during superplastic strain of the UFG Al–Mg–Sc–Zr alloys.

In order to practically apply the UFG alloys, it is necessary to provide a maximum possible degree of uniform strain during superplastic punching. In order to describe causes of loss of strength during superplasticity of the UFG alloys, one can use a Hart approach [23] based on representations about termination of the stable uniform plastic flow with insufficient rate or strain hardening that are characterized coefficients m and n, respectively. Efficiency of application of this approach was previously demonstrated in the study [30]. According to the Hart criterion, the condition of termination of the stable plastic flow of the material in tensioning can be represented as follows [42]:

$$m + n/\varepsilon \geq 1, \tag{3}$$

where m is a rate sensitivity coefficient of the flow stress in the equation (1), $n = \partial \ln(\sigma)/\partial \ln(\varepsilon)$ is a strain hardening coefficient.

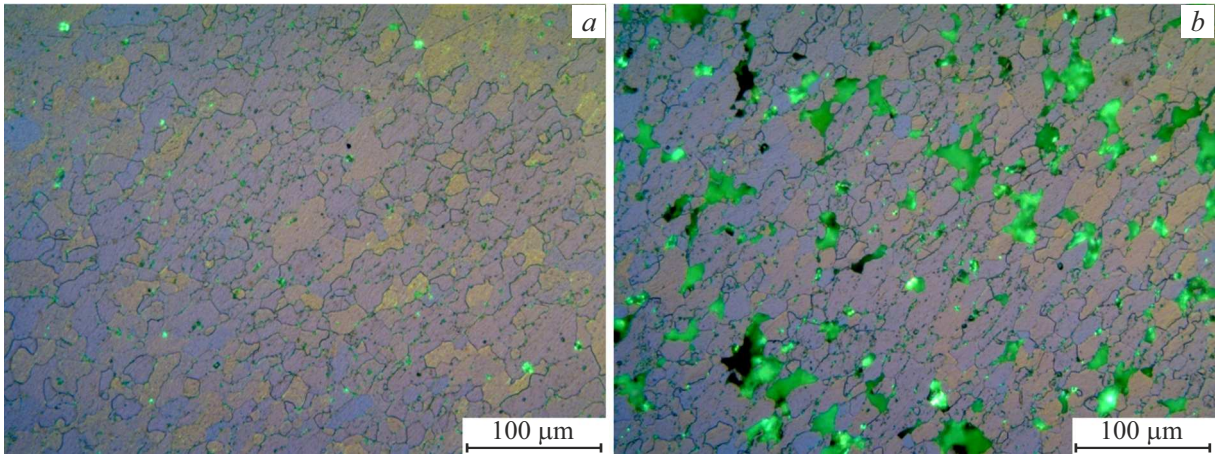

Figure 10. Microstructure of the unstrained (a) and strained (b) area of the samples of the Al−4% Mg−0.22% Sc−0.10% Zr alloys after the SP tests ($T = 500\,^{\circ}$C, $\dot{\varepsilon} = 3.3 \cdot 10^{-3}\,\mathrm{s}^{-1}$). Metallography. Interference contrast.

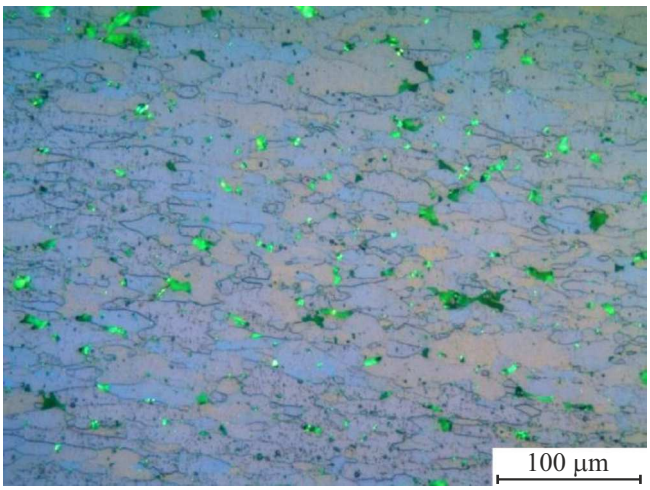

Figure 11. Microstructure of the strained area of the sample of the Al−4% Mg−0.22% Sc−0.10% Zr alloy after the SP tests when $T = 500\,^{\circ}$C and the strain rate $\dot{\varepsilon} = 3.3 \cdot 10^{-1}\,\mathrm{s}^{-1}$. Metallography. Interference contrast.

The plastic flow of the material will remain to be uniform up to reaching the strain degree ε_1:

$$\varepsilon_1 \leq n/(1-m). \qquad (4)$$

Consequently, using experimental data about values of the coefficients n and m, on can determine strain ε_1, at which localization of the plastic flow starts and the curve $\sigma_t(\varepsilon_t)$ originates the loss-of-strength stage. As said above, in order to determine values of m, n and ε_1, the dependences „engineering stress (σ) — engineering strain (ε)“ are recalculated into the dependences „true stress (σ_t) — true strain (ε_t)“ according to the study [33] (Fig. 12).

Strain hardening stage

A value of the strain hardening coefficient $n = \partial \ln(\sigma_t)/\partial \ln(\varepsilon_t)$ characterizes susceptibility of the material to uniform strain (see the study [31]). This value can be determined by a slope angle of the curves $\sigma_t(\varepsilon_t)$ in the logarithmic coordinates $\ln(\sigma_t) - \ln(\varepsilon_t)$.

Fig. 13 shows the dependences $\sigma_t(\varepsilon_t)$ in the coordinates $\ln(\sigma_t) - \ln(\varepsilon_t)$ for the UFG alloys with 0.22 % Sc + 0.10 % Zr (Fig. 13, *a,c*) and with 0.10 % Sc−0.22 % Zr (Fig. 13, *b,d*). For the alloys with the low magnesium content, the dependences $\ln(\sigma_t) - \ln(\varepsilon_t)$ have a pronounced two-stage nature — the stage of intense strain hardening, which is characterized by the high coefficient $n = n_1$, which is replaced by the stage with the low coefficient n_2. The strain hardening coefficient n_2 weakly depends on the strain temperature and the magnesium concentration. The value of the coefficient n_1 in the alloys with 2.5 % and 4 % Mg increases with an increase of the temperature of strain. The increase of the Sc concentration in the alloys with 2.5 % or 4 % Mg (the increase of the Sc/Zr ratio) results in an increase of the coefficient n_2.

In the alloys with 6 % Mg, the two-stage nature of strain hardening is observed only for the low strain temperatures (300 °C−350 °C); at the temperatures 400 °C−500 °C the curve $\sigma_t(\varepsilon_t)$ in the logarithmic coordinates $\ln(\sigma_t) - \ln(\varepsilon_t)$ with good accuracy ($R^2 > 0.9$) can be interpolated by a straight line (Fig. 13, *c,d*). At the elevated temperatures, duration of the stage of intense strain hardening becomes very small and $n \sim n_2$.

According to the model [43], the value of the coefficient n in the UFG materials depends on a nature and value of fields of long-rang stresses that occur in the material during superplastic strain. In the UFG materials, the value of the long-range fields of internal stress (σ_i) is mainly contributed by defects that hit the grain boundaries during plastic strain [43,44]. The long-range fields of the internal stresses σ_i from the non-equilibrium grain boundaries prevent motion of lattice dislocations. According to the study [44], the magnitude σ_i depends on a density ρ_b of orientation mismatch dislocations (OMD) distributed within the boundaries and a density of a

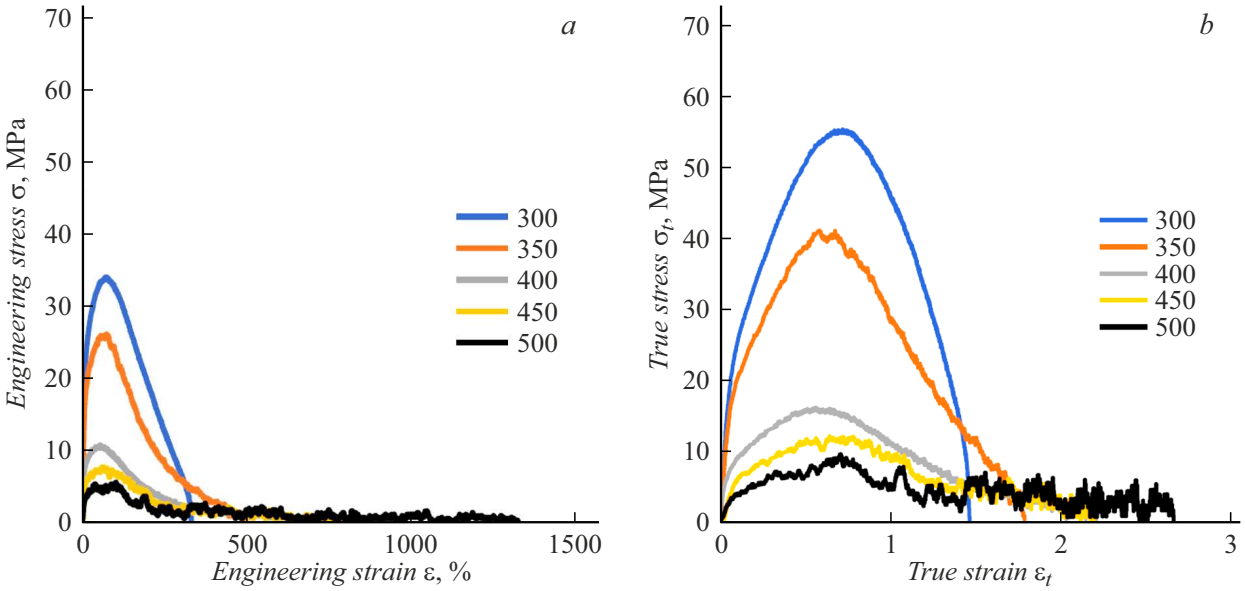

Figure 12. Tensile curves of the samples of the Al–2.5% Mg–0.16% Sc–0.16% Zr alloy in the coordinates „engineering stress — engineering strain" (*a*) and „true stress — true strain" (*b*). The strain rate is $\dot{\varepsilon} = 3.3 \cdot 10^{-3}\,\mathrm{s}^{-1}$. The temperatures in legends in the graphs are given in °C.

Burgers vector w_t of sliding components of the delocalized dislocations: $\sigma_i = \varphi_1 G\rho_b\Delta b + \varphi_2 G w_t$, where φ_1, φ_2 are numerical coefficients. (Hereinafter, the density of the Burgers vector of a dislocation shall be understood as a tensor a_{ki}, which makes it possible to represent the Burgers vector b as an integral over a surface S that rests on a contour L: $b_i = \int_S a_{ki} dS_k$.)

In case when $\rho_b\Delta b \gg w_t$, a dependence of the strain hardening rate on the strain rate is expressed as follows

$$\dot{\bar{\sigma}} = \xi\dot{\varepsilon}_v - \bar{\sigma}^4[D_b\delta G/A_1 kT]\exp(\varphi_1\bar{\sigma}/\alpha_b w_0), \qquad (5)$$

where $\bar{\sigma} = \sigma/G\varphi$, $A_1 = 50$ is a numerical coefficient, $\dot{\varepsilon}_v$ is an intragranular strain rate, ξ is a coefficient that characterizes homogeneity of a dislocation flux, $w_0 = 0.5$, $\alpha_b \sim 0.02$ at $0.5T_m$ (T_m is a melting temperature in K), D_b is a grain-boundary diffusion coefficient, δ is a grain boundary width [43].

When $w_t \ll \rho_b\Delta b$, the equation for calculating the strain hardening rate can be written as

$$\dot{\bar{\sigma}} = \xi\dot{\varepsilon}_v - \bar{\sigma}^2[(b/d)^2 D_b\delta G C_1/kT]\exp(\varphi_2\bar{\sigma}/\alpha_b w_0), \qquad (6)$$

where $C_1 = 10$ is a numerical coefficient [43].

The first summand in the equations (5) and (6) describes kinetics of defect accumulation in a grain boundary ($I^+ = \xi\dot{\varepsilon}_v/b$), while the second thereof describes kinetics of their removal from the grain boundaries due to progress of processes of return or growth of the grains ($I^- = \rho_b\Delta b/t_1$ or $I^- = w_t/t_2$, where t_1 and t_2 is a time of delocalization of the OMDs and the sliding components of the delocalized dislocations, respectively). It is clear from the equations (5), (6) that the nature of strain hardening will be different in cases when $\rho_b\Delta b \gg w_t$ and $w_t \ll \rho_b\Delta b$. It follows from comparing the formulas (5) and (6) that in a case when the OMDs prevail in the grain boundaries ($\rho_b\Delta b \gg w_t$), the value of the strain hardening coefficient turns out to be less than in a case when $w_t \ll \rho_b\Delta b$ (when $d = \mathrm{const}$).

In this regard, the two-stage nature of strain hardening during superplasticity of the UFG alloys is primarily related to a various type of defects accumulated at the grain boundaries (see [45,46]).

A large slope angle of the curves $\sigma_t(\varepsilon_t)$ in the logarithmic coordinates $\ln(\sigma_t) - \ln(\varepsilon_t)$ at the first stage of strain hardening (the large value of the strain hardening coefficient $n_1 > n_2$) is induced, in our opinion, by accumulation of the sliding components of the Burgers vector of the delocalized dislocations at the grain boundaries of the UFG alloys. The increased density of the gliding components of the Burgers vector of the delocalized dislocations ($w_t \gg \rho_b\Delta b$) is related to intense delocalization of the OMDs that hit the grain boundaries of the UFG alloys at the ECAP stage. Truth of this assumption is confirmed by an increase of the slope angle of the curves $\ln(\sigma_t) - \ln(\varepsilon_t)$ in the UFG alloys with 2.5 % Mg when the strain temperature increases (Fig. 13, *a,b*). As said above, the increase of the Mg concentration results in reduction of the grain-boundary diffusion coefficient and the increase of energy of grain-boundary diffusion activation (see [22,23]). The increased magnesium concentration in the UFG Al–6% Mg–Sc–Zr alloys results in reduction of intensity of the OMD delocalization process and, consequently, a decrease of the density of the Burgers vector of the delocalized dislocations. As a result, in the UFG alloys with 6 % Mg a case when $\rho_b\Delta b \gg w_t$ is

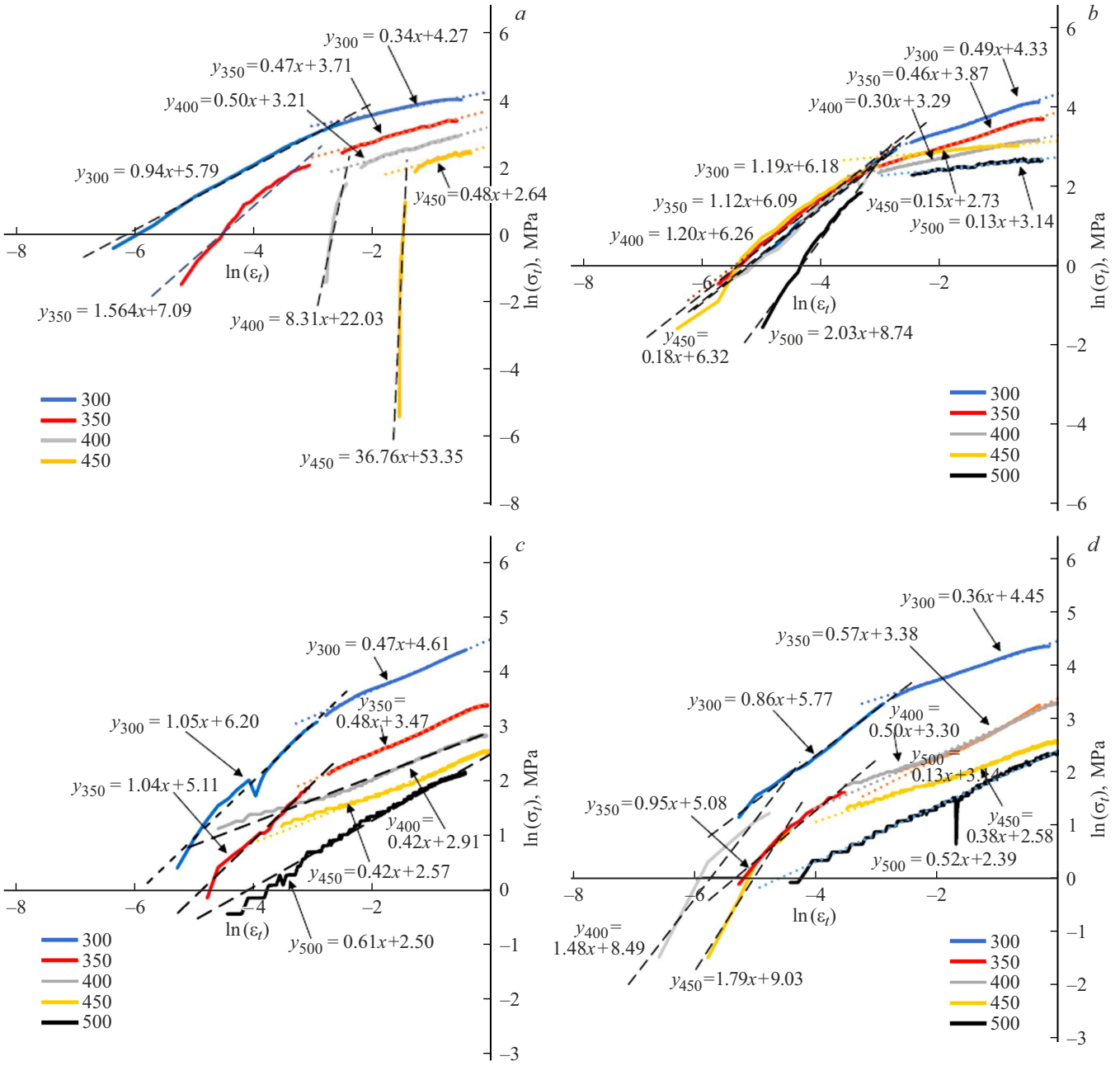

Figure 13. Analysis of the strain hardening stage for the alloys with 2.5 % Mg *(a,b)* and 4 % Mg *(c,d)* and with the various content of Sc and Zr: *a,c* — Sc/Zr = 2.2; *b,d* — Sc/Zr = 0.45. $\dot{\varepsilon} = 3.3 \cdot 10^{-3}\,\mathrm{s}^{-1}$. The temperatures in legends in the graphs are given in °C.

realized, which is characterized by small values of the strain hardening coefficient ($n \sim n_2$).

It is important to note that at the elevated temperatures (450 °C–500 °C) the curves $\sigma_t(\varepsilon_t)$ exhibit a surge-like change of stresses, which indicates a progress of dynamic recrystallization during superplasticity of the UFG alloys (see [4,5]). The grain growth during dynamic recrystallization can additionally result in reduction of the density of defects at the grain boundaries and, consequently, reduction of the fields of internal stresses. It will also contribute to reduction of the strain hardening coefficient during superplasticity of the UFG alloys.

Stage of stationary flow

The key characteristic that describes the stage of stationary superplastic flow of the fine-grained alloys is the rate sensitivity coefficient of the flow stress $m = \ln(\sigma_y)/\ln(\dot{\varepsilon})$ [31]. Under the optimal temperature-rate conditions of superplastic strain, the coefficient $m \to 0.5$ [31]. In these conditions, the superplastic strain rate ($\dot{\varepsilon} = \dot{\varepsilon}_v + \dot{\varepsilon}_b$) is

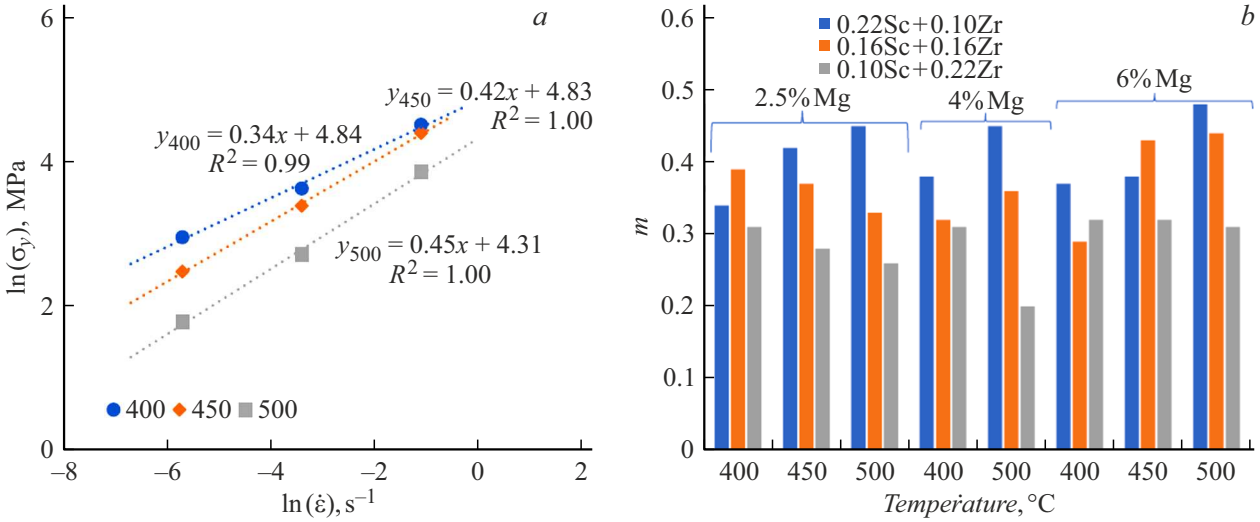

Figure 14. Analysis of rate sensitivity of the flow stress during superplastic strain of the fine-grained alloys: *a* — the dependence of the flow stress on the strain rate in the coordinates $\ln(\sigma_y) - \ln(\dot{\varepsilon})$ for the Al–2.5% Mg–0.22% Sc–0.10% Zr alloy; *b* are values of the coefficient *m* for the alloys with the various Mg concentration and Sc/Zr ratio.

Table 2. Experimental (ε^*) and theoretical values (ε_1) of the magnitude of limit uniform strain during superplasticity of the UFG alloys

T, °C	$\dot{\varepsilon}$, s^{-1}	ε	Al–2.5% Mg			Al–4% Mg			Al–6% Mg [30]		
			Sc/Zr=2.2	Sc/Zr=1.0	Sc/Zr=0.45	Sc/Zr=2.2	Sc/Zr=1.0	Sc/Zr=0.45	Sc/Zr=2.2	Sc/Zr=1.0	Sc/Zr=0.45
400	$3.3\cdot10^{-3}$	ε^*	0.66±0.05	0.59±0.04	0.69±0.05	0.99±0.05	0.82±0.06	0.91±0.06	0.90±0.08	1.0±0.1	1.1±0.1
		ε_1	0.76	0.56	0.43	0.58	0.72	0.49	0.78	0.66	0.70
	$3.3\cdot10^{-2}$	ε^*	0.62±0.04	0.63±0.08	0.7±0.1	0.84±0.05	0.74±0.07	0.73±0.06	1.0±0.1	1.0±0.1	0.94±0.08
		ε_1	0.55	0.62	0.61	0.71	0.66	0.51	0.74	0.69	0.55
	$3.3\cdot10^{-1}$	ε^*	0.55±0.04	0.62±0.08	0.54±0.08	–	–	0.58±0.05	0.88±0.06	0.83±0.06	0.75±0.06
		ε_1	0.52	0.48	0.36			0.22	0.69	0.76	0.55
450	$3.3\cdot10^{-3}$	ε^*	0.72±0.05	0.69±0.04	0.50±0.03	–	–	–	1.0±0.1	1.0±0.1	1.0±0.1
		ε_1	0.83	0.57	0.18				0.70	0.86	0.62
	$3.3\cdot10^{-2}$	ε^*	0.72±0.06	0.74±0.08	0.7±0.1	–	–	–	1.0±0.1	1.0±0.1	1.00±0.09
		ε_1	0.74	0.67	0.28				0.82	0.75	0.73
	$3.3\cdot10^{-1}$	ε^*	0.56±0.06	0.61±0.04	0.52±0.08	–	–	–	0.77±0.06	0.80±0.06	0.78±0.06
		ε_1	0.52	0.52	0.36				0.73	0.86	0.52
500	$3.3\cdot10^{-3}$	ε^*	0.9±0.1	0.74±0.07	0.57±0.04	0.77±0.08	1.2±0.1	1.1±0.1	0.99±0.08	1.0±0.1	1.1±0.1
		ε_1	0.80	0.57	0.20	0.69	0.78	0.58	0.97	0.64	0.79
	$3.3\cdot10^{-2}$	ε^*	0.74±0.08	0.79±0.09	0.56±0.09	1.0±0.1	0.86±0.05	0.73±0.07	1.0±0.1	1.0±0.1	1.05±0.09
		ε_1	0.76	0.78	0.20	0.96	0.72	0.39	0.78	0.71	0.68
	$3.3\cdot10^{-1}$	ε^*	0.70±0.08	0.68±0.06	0.53±0.05	–	–	0.71±0.03	1.1±0.1	0.80±0.06	0.88±0.08
		ε_1	0.76	0.66	0.20			0.36	0.81	0.88	0.58

mainly contributed by the grain boundary sliding process ($\dot{\varepsilon}_b$), while a contribution by intragranular strain ($\dot{\varepsilon}_v$) is very small.

A value of the coefficient *m* can be determined by the slope angle of the dependence of the flow stress on the strain rate in the logarithmic coordinates $\ln(\sigma_y) - \ln(\dot{\varepsilon})$ (Fig. 14, *a*). For all the dependences $\ln(\sigma_y) - \ln(\dot{\varepsilon})$, a coefficient of confidence of linear correlation $R^2 > 0.95$. It indicates that the superplastic strain mechanism does not vary within the studied range of the strain rates (from $3.3 \cdot 10^{-3}$ to $3.3 \cdot 10^{-1}$ s^{-1}).

Fig. 14, *b* shows results of calculations of the value of the coefficient *m* for the alloys with the various content of Mg, Sc and Zr at the temperatures of 400 °C, 450 °C and 500 °C.It is clear in Fig. 14, *b* that for the alloys with the increased Sc content there is an observed increase of the co-

efficient m when the temperature of strain increases. At the temperature of 500 °C, in the UFG alloys with Sc/Zr = 2.2, the coefficient $m \sim 0.45-0.48$. This value is very close to the optimal $m \sim 0.5$, thereby indicating a prevailing contribution by grain boundary sliding to the stable superplastic flow of the fined-grained material. The Mg concentration does not significantly affect the coefficient m in the alloys with Sc/Zr = 2.2 (Fig. 14, *b*). In the alloys with the increased zirconium content and the low magnesium content (2.5 %, 4 % Mg), the increase of the test temperature results in reduction of the coefficient m. In particular, with an increase of the test temperature from 400 °C to 500 °C for the Al−2.5% Mg−0.10% Sc−0.22% Zr alloy the coefficient m decreases from 0.31 to 0.26, and from 0.31 to 0.20 in the UFG Al−4% Mg−0.10% Sc−0.22% Zr alloy. The alloys with 6 % Mg and the increased zirconium content do not exhibit a pronounced dependence of the coefficient m on the test temperature. The low values of the coefficient m in the alloys with the increased zirconium content indicate that the contributions by grain boundary sliding and intragranular sliding are comparable.

Loss-of-strength stage

As shown above, according to the Hart criterion [42], when reaching the critical strain degree ε_1, the loss-of-strength stage starts. Let us calculate a value of the critical strain degree ε_1 and compare it with the experimental value ε^*, which is determined based on analysis of the curves „true stress — true strain". A large error of determination of the value ε^* at the temperatures 450 °C−500 °C ($\Delta\varepsilon^* = 0.10-0.12$) is related to presence of the long uniform-flow state as well as to the surge-like change of the stress due to evolution of the dynamic recrystallization processes. Results of calculations of the value of ε_1 and comparison with the experimental data (ε^*) are shown in Table 2. When calculating the value of ε_1 according to the formula (4), a value of the strain hardening coefficient was assumed to be $n = n_2$, while a value of the coefficient m was assumed to be the same for all the strain rates (from $3.3 \cdot 10^{-3}$ to $3.3 \cdot 10^{-1}\,s^{-1}$ when $T = \text{const}$).

The best agreement of the calculation results with the experimental data is achieved for the alloys with the increased Sc content. For the alloys with the increased zirconium content, there is an observed significant difference between the values of ε^* and ε_1. In our opinion, a key reason of the observed differences can be discontinuous decomposition of a solid solution in the alloys with Sc/Zr = 0.45 as well as fast cavitational failure of these alloys due to precipitation of the coarse fusiform Al_3Zr particles.

According to the model [47], pore formation is caused by accumulation of defects on the second-phase particles. Under the SP conditions, the pores are formed on the second-phase particles arranged in triple junctions of the grains. In the first approximation, a defect that is formed on the particle of the radius R, which is arranged in the grain boundary, can be described as a disclinational loop of the radius R and power $\omega(t)$. The disclinational loop power $\omega(t)$ increases in proportion to a number of defects that hit the boundary at the speed $\dot{\varepsilon}_v$: $\omega(t) = \varphi_1 \dot{\varepsilon}_v t$ [47,48], where φ_3 is a numerical coefficient. As the defects are accumulated on the grain boundaries, the disclinational loop power $\omega(t)$ increases and elastic energy related to this defect increases as well. When reaching the critical power ω^*, an excessive loop power is so high that it is energetically favorable for the grain boundary to „dump" a source of this energy. At the increased temperatures, the stored energy will be relaxed by formation of micropores, whose growth rate is proportional to a degree and rate of intragranular strain. We note that the coarse Al_3X particles often cause cavitational failure during superplasticity of the fine-grained aluminum alloys [30,49,50].

3.2. Effect of the Sc and Zr ratio

Anticipating the analysis, it is important to note that an atomic mass of zirconium (91.224 amu) is almost in two times higher that an atomic mass of scandium (44.96 amu). Therefore, partial replacement of Sc with a mass-equivalent content of Zr will result in reduction of the volume portion of the precipitating $Al_3(Sc,Zr)$ particles. The increased volume portion of the $Al_3(Sc,Zr)$ particles in the UFG alloys with Sc/Zr = 1 and 2.2 is one of the important factors for providing high superplastic characteristics of these alloys. Under the other similar conditions, the large volume portion of the $Al_3(Sc,Zr)$ particles makes it possible to provide a smaller grain size and, consequently, the larger elongation to failure and the lower flow stress in the UFG alloys.

As shown above, when the alloys with the increased scandium content (Sc/Zr = 2.2) are heated, the spherical Al_3Sc nanoparticles precipitate. When the alloys with the increase zirconium content (Sc/Zr = 0.45) are heated, within the grain volume the nanoparticles Al_3Sc and $Al_3(Sc_{0.5}Zr_{0.5})$ precipitate and near the grain boundaries the fusiform submicron Al_3Zr particles precipitate by the discontinuous decomposition mechanism. It affects, first of all, the grain growth and the nature of failure of the fine-grained alloys. We note that, in turn, the grain growth affects stability of the SP flow and maximum elongation to failure of the fine-grained alloys.

As it is known, specifics of the Al_3Sc particles are fast formation and a fast growth at the elevated temperatures of heating. As a result, the Al_3Sc particles provide effective stabilization of the non-equilibrium UFG microstructure at the low heating temperatures, but are not effective stoppers for migrating grain boundaries at the high temperatures of heating or strain.

The $Al_3(Sc_{0.5}Zr_{0.5})$ particles have a structure „a Al_3Sc core— a Al_3Zr shell" [51,52], which provides a good combination of fast precipitation at the low temperature and a low growth rate at the increased temperatures of heating or strain. As a result, the Al−Mg−Sc−Zr alloys with Sc/Zr ≥ 1 demonstrate higher mechanical properties and SP characteristics at the elevated temperatures.

The fusiform Al_3Zr particles formed by the discontinuous decomposition mechanism adversely affect maximum plasticity of the fine-grained aluminum alloys — these particles cause formation of large pores and premature cavitational failure of the aluminum alloys [30,53]. Formation of the Al_3Zr particles by the discontinuous decomposition mechanism is, in our opinion, one of the key reasons of plasticity reduction at the elevated temperatures of strain of the alloys with the low magnesium content and the low ratio $Sc/Zr = 0.45$ (Table 1, Fig. 7, *a*). The coarse Al_3Zr particles do not allow effectively stabilizing the non-equilibrium UFG microstructure of the alloys, thereby resulting in formation of the coarse recrystallized grains in the alloys with the low magnesium content (Fig. 4). The grain growth also results in reduction of plasticity of the Al–Mg–0.10% Sc–0.22% Zr alloys with 2.5 % and 4 % Mg (Table 1). The slight increase of plasticity of the Al–6% Mg–0.10% Sc–0.22% Zr alloys is related to the effect of magnesium on the grain-boundary diffusion coefficient (D_b) aluminum — reduction of D_b makes it possible to decrease the grain growth rate ans partially compensate a weak influence of the coarse Al_3Zr particles on migration mobility of the grain boundaries of the UFG aluminum.

Let us analyze the effect of the Sc/Zr ratio on the superplastic characteristics of the fine-grained aluminum alloys. As it is clear from Fig. 7, *f*, at 500 °C maximum plasticity is observed in the alloys with $Sc/Zr = 1$. The alloys with $Sc/Zr = 2.2$ and $Sc/Zr = 0.45$ have lower plasticity under the similar temperature-rate conditions of strain. In our opinion, it is related to the fact that the alloys with $Sc/Zr = 1$ have the minimum number of the Al_3Zr particles that contribute to intense cavitational failure and a large number of stable $Al_3(Sc_{0.5}Zr_{0.5})$ nanoparticles with the structure „the Al_3Sc core— the Al_3Zr shell“. When heating the alloys with $Sc/Zr = 2.2$, the Al_3Sc particles quickly grow and, therefore, the grains quickly grow, thereby preventing from providing the high SP properties of the Sc-enriched alloys. When the Zr-enriched alloys are heated, the coarse Al_3Zr particles are formed, which facilitate cavitational failure of the fine-grained alloys and limit their plasticity at the elevated temperatures (450 °C–500 °C). We also note that the Zr-enriched alloys exhibit an anomalous grain growth that contributes to reduction of plasticity of the alloys with $Sc/Zr = 0.45$. The low volume portion of the coarse Al_3Zr particles at the decreased temperatures (400 °C and less) as well as the large volume portion and the low growth rate of the Al_3Sc particles make it possible to provide increased plasticity of the UFG alloys with the ratio $Sc/Zr = 2.2$ (Fig. 7, *e*).

We note that in case of suppression of discontinuous decomposition of the solid solution the Zr-enriched alloys can have a further increase of their superplastic characteristics. One of the effective methods of reduction of intensity of discontinuous decomposition of the solid solution can be two-stage heat treatment of the Zr-enriched alloys (see, for example, [34,35]). It will make it possible to provide further reduction of expensive scandium in the composition of the Al–Mg–Sc–Zr aluminum alloys.

3.3. Effect of magnesium

It should be preliminarily noted that the Sp tests were performed within the temperature interval 300 °C–500 °C.As it is clear from Table 1, the best results (the maximum values of elongation to failure) are obtained at the temperatures 450 °C–500 °C that exceed a temperature of dissolving of the β-phase particles in the Al–Mg alloys (see, for example, [54]). Therefore, we did not take into account the effect of the β-phase particles on the superplastic behavior of the UFG Al–Mg–Sc–Zr alloys in optimal strain modes. When analyzing the results, the main focus was on the effect of the Mg concentration in the solid solution on the superplastic behavior of the UFG Al–Mg–Sc–Zr alloys.

The effect of the β-phase particles can be expected in case of strain at the decreased temperatures (300 °C, 350 °C). According to the study [55], the β-phase particles can contribute to recrystallization during plastic strain and increase the degree of homogeneity of the grain structure in the Al–Mg alloys. Besides, the submicron β-phase particles can provide an increase of the flow stress and contribute to more intense strain hardening of the UFG Al–Mg alloys (as compared to the hardened Al–Mg alloys, in which magnesium is mainly in the solid solution).

The results of the SP tests are analyzed to show that the increase of the Mg concentration up to 6 % results in simultaneous reduction of relative elongation to failure and the flow stress of the fine-grained alloys (Fig. 7, *e*,*f*). It is a quite unexpected result, since according to the structural superplasticity theory [31,32] it is usually assumed that the fine-grained materials with high plasticity shall be characterized by minimum values of the flow stress. Since the maximum plasticity ($\delta_{\max}$) is observed in the alloys with 2.5 % Mg (Fig. 7, *e*,*f*), then it would be expected that the minimum flow stresses (σ_y) will also be observed in the alloys with 2.5 % Mg.

In our opinion, the observed effect is mainly caused by an intense progress of dynamic recrystallization in the fine-grained alloys with the decreased magnesium content. As it is clear from Fig. 7, *a*–*d*, the strain curves $\sigma(\varepsilon)$ of the alloys with 2.5 % Mg exhibit high stress surges; with the increase of the Mg concentration a scope of the surge-like change of stresses becomes much smaller. As it is known, the dynamic recrystallization process is accompanied by formation of a variously-grained microstructure [30,56–58].

It is known that magnesium results in reduction of the grain-boundary diffusion coefficient (D_b) in aluminum [22,23] and, consequently, reduction of a ratio of migration of the grain boundaries under the SP conditions:

$$V_m = A_\rho C_b (\sigma/G)(b/d)b, \tag{7}$$

where $A_\rho = 2\pi/\ln(d/b)$, $C_b = D_b(G\delta/kT)$ [44].

Formation of a more fine-grained microstructure in the alloys with 6 % Mg results in reduction of the flow stress

according to the study [43] (see also the equation (6)). Besides, as noted above (see Section 3.2), reduction of D_b and the increase of stability of the UFG microstructure can partially compensate the adverse effect of the coarse Al_3Zr particles that are formed by the discontinuous precipitation mechanism.

Conclusions

1. The tensile curves $\sigma(\varepsilon)$ of the alloys with 2.5 % Mg are characterized by the surge-like change of the stress, thereby indicating the progress of the dynamic recrystallization processes. The increase of the Mg concentration results in reduction of the scope of the stress surges. At the high strain degrees ($\varepsilon > 700\,\%-800\,\%$), the curves $\sigma(\varepsilon)$ exhibit the stress increasing stage that indicates an intense progress of the strain-induced grain growth. This conclusion is confirmed by the results of the studies of the alloy microstructure after the SP tests.

2. The process of strain hardening of the fine-grained $Al-(2.5,4)\%\,Mg-Sc-Zr$ alloys is of the two-stage nature due to replacement of the mechanism of defect accumulation at the grain boundaries. At the low strain degrees, the curves $\sigma(\varepsilon)$ are characterized by the high strain hardening coefficient, whose value is determined by the rate of accumulation of the sliding components of the delocalized dislocations at the grain boundaries. At the elevated temperatures and strains, the strain hardening coefficient of the fine-grained alloys is sharply reduced and orientation mismatch undelocalized dislocations start prevailing at the grain boundaries.

3. The stage of stationary flow of the fine-grained alloys is characterized by high values of the rate sensitivity coefficient — at the temperature of 500 °C in the alloys with $Sc/Zr = 2.2$ the coefficient $m \sim 0.45-0.48$. In the alloys with the increase zirconium content and the low magnesium content (2.5 %, 4 % Mg), the increase of the test temperature results in reduction of the coefficient m to $\sim 0.20-0.31$. The high values of the coefficient m indirectly indicate that the grain boundary sliding rate predominantly contributes to the total superplastic strain rate.

4. The increase of the magnesium concentration results in reduction of the superplastic characteristics of the fine-grained alloys (when $Sc/Zr = \text{const}$). With the strain temperature of 500 °C and the strain rate of $3.3 \cdot 10^{-2}\,s^{-1}$, elongation to failure reaches $\delta_{max} = 1970\,\%$ in the $Al-2.5\%\,Mg-0.22\%\,Sc-0.10\%\,Zr$ alloy and $\delta_{max} = 1750\,\%$ in the $Al-2.5\%\,Mg-0.16\%\,Sc-0.16\%\,Zr$ alloy. Under the similar temperature-rate conditions of strain, elongation to failure is 400 % in the $Al-6\%\,Mg-0.22\%\,Sc-0.10\%\,Zr$ alloy and $\delta_{max} = 1215\,\%$ in the $Al-6\%\,Mg-0.16\%\,Sc-0.16\%\,Zr$ alloy. For the alloys with $Sc/Zr \geq 1$, good compliance of the Hart criterion is observed for estimating the maximum degree of uniform strain. It is shown that the Mg effect first of all consists of the increase of stability of the non-equilibrium fine-grained microstructure of the aluminum alloys and of reduction of the grain growth rate during superplasticity.

Acknowledgments

The authors would like to thank V.V. Zakharov (JSC „VILS“, Moscow) for his recommendations for selecting alloy compositions and their casting modes. The TEM studies were performed by N. Yu. Tabachkova using equipment of „Materials Science and Metallurgy“ Common Use Center of NUST „MISIS“. The authors would like to thank A.V. Piskunov (UNN, Moscow) for assistance in developing a procedure of the metallographic study of the samples after the superplasticity tests.

Funding

The study was supported financially by the Russian Science Foundation (grant №. 22-13-00149) and the Ministry of Education and Science of Russia (project №. 075-03-2023-096 (FSWR-2023-0037)).

Conflict of interest

The authors declare that they have no conflict of interest.

References

[1] V.G. Davydov, T.D. Rostova, V.V. Zakharov, Y.A. Filatov, V.I. Yelagin. Mater. Sci. Eng. A, **280**, 30 (2000). DOI: 10.1016/S0921-5093(99)00652-8
[2] Y.A. Filatov, V.I. Yelagin, V.V. Zakharov. Mater. Sci. Eng. A, **280**, 97 (2000). DOI: 10.1016/S0921-5093(99)00673-5
[3] E. Avtokratova, O. Sitdikov, M. Markushev, R. Mulyukov. Mater. Sci. Eng. A, **538**, 386 (2012). DOI: 10.1016/j.msea.2012.01.041
[4] R. Kaibyshev, E. Avtokratova, A. Apollonov, R. Davies. Scr. Mater., **54**, 2119 (2006). DOI: 10.1016/j.scriptamat.2006.03.020
[5] Y.B. Sun, X.P. Chen, J. Xie, C. Wang, Y.F. An, Q. Liu. Mater. Today Comm., **33**, 104217 (2022). DOI: 10.1016/j.mtcomm.2022.104217
[6] F. Musin, R. Kaibyshev, Y. Motohashi, G. Itoh. Metall Mater. Trans. A, **35**, 2383 (2004). DOI: 10.1007/s11661-006-0218-4
[7] E. Avtokratova, O. Sitdikov, M. Markushev. Lett. Mater., **5** (3), 319 (2015). DOI: 10.22226/2410-3535-2015-3-319-323
[8] V.N. Perevezentsev, M.Y. Shcherban', M.Y. Murashkin, R.Z. Valiev. Tech. Phys. Lett., **33** (8), 648 (2007). DOI: 10.1134/S106378500708007X
[9] T.G. Nieh, L.M. Hsiung, J. Wadsworth, R. Kaibyshev. Acta Mater., **46** (8), 2789 (1998). DOI: 10.1016/S1359-6454(97)00452-7
[10] T.G. Nieh, R. Kaibyshev, L.M. Hsiung, N. Nguyen, J. Wadsworh. Scr. Mater., **36** (9), 1011 (1997). DOI: 10.1016/S1359-6462(96)00479-4
[11] Y.L. Duan, L. Tang, Y. Deng, X.W. Cao, G.F. Xu, Z.M. Yin. Mater. Sci. Eng. A., **669**, 205 (2016). DOI: 10.1016/j.msea.2016.05.086

[12] Y.-Y. Li, W.-H. Wang, Y.-F. Hsu, S. Trong. Mater. Sci. Eng. A, **497** (1–2), 10 (2008). DOI: 10.1016/j.msea.2008.08.019
[13] Y. Duan, G. Xu, L. Tang, Y. Liu, J. Xu, Y. Deng, Z. Yin. J. Alloys Compd., **715**, 311 (2017). DOI: 10.1016/j.jallcom.2017.04.273
[14] G. Xu, X. Cao, T. Zhang, Y. Duan, X. Peng, Y. Deng, Z. Yin. Mater. Sci. Eng. A, **672**, 98 (2016). DOI: 10.1016/j.msea.2016.06.070
[15] O. Sitdikov, E. Avtokratova, O. Latypova, M.V. Markushev. Lett. Mater., **8** (4s), 561 (2018). DOI: 10.22226/2410-3535-2018-4-561-566
[16] F.C. Liu, Z.Y. Ma, L.Q. Chen. Scr. Mater., **60**, 968 (2009). DOI: 10.1016/j.scriptamat.2009.02.021
[17] F.C. Liu, P. Xue, Z.Y. Ma. Mater. Sci. Eng. A, **547**, 55 (2012). DOI: 10.1016/j.msea.2012.03.076
[18] F.C. Liu, Z.Y. Ma. Scr. Mater., **59** (8), 882 (2008). DOI: 10.1016/j.scriptamat.2008.06.035
[19] F.C. Liu, Z.Y. Ma, F.C. Zhang. J. Mater. Sci. Technol., **28** (11), 1025 (2012). DOI: 10.1016/S1005-0302(12)60168-6
[20] M. Li, Q. Pan, Y. Shi, X. Sun, H. Xiang. Mater. Sci. Eng. A, **687**, 298 (2017). DOI: 10.1016/j.msea.2017.01.091
[21] K. Wang, F.C. Liu, P. Xue, D. Wang, B.L. Xiao, Z.Y. Ma. Metall. Mater. Trans. A, **47**, 546 (2016). DOI: 10.1007/s11661-015-3230-8
[22] T. Fujita, Z. Horita, T.G. Langdon. Phil. Mag. A, **82**, 2249 (2002). DOI: 10.1080/01418610208235736
[23] X. Sauvage, N. Enikeev, R. Valiev, Y. Nasedkina, M. Murashkin. Acta Mater., **72**, 125 (2014). DOI: 10.1016/j.actamat.2014.03.033
[24] H. Hasegawa, S. Komura, A. Utsunomiya, Z. Horita, M. Furukawa, M. Nemoto, T.G. Langdon. Mater. Sci. Eng. A, **265**, 188 (1999). DOI: 10.1016/S0921-5093(98)01136-8
[25] C.-R. Song, B.-X. Dong, S.-Y. Zhang, H.-Y. Yang, L. Liu, J. Kang, J. Meng, C.-J. Luo, C.-G. Wang, K. Cao, J. Qiao, S.-L. Shu, M. Zhu, F. Qiu, Q.-C. Jiang. J. Mater. Res. Technol., **31**, 3255 (2024). DOI: 10.1016/j.jmrt.2024.07.051
[26] N.P. Lyakishev. *Diagrammy sostoyaniya dvoinykh metallicheskikh sistem:* spravochnik (Mashinostroenie, M., 1996) (in Russian).
[27] V.S. Sinyavskii, V.D. Val'kov, E.V. Titkova. Zashchita metallov, **34** (6), 613 (1998) (in Russian).
[28] V.V. Zakharov, I.A. Fisenko. Metal Sci. Heat Treatment, **61** (3–4), 217 (2019). DOI: 10.1007/s11041-019-00403-4
[29] V.V. Zakharov, Yu.A. Filatov. Tekhnologiya legkikh splavov, **4**, 21 (2021) (in Russian). DOI: 10.24412/0321-4664-2021-4-31-37
[30] V.N. Chuvil'deev, M.Yu. Gryaznov, S.V. Shotin, A.V. Nokhrin, C.V. Likhnitskii, G.S. Nagicheva, M.K. Chegurov, V.I. Kopylov, A.A. Bobrov, I.S. Shadrina. Mater. Sci. Eng. A, **898**, 146409 (2024). DOI: 10.1016/j.msea.2024.146409
[31] T.G. Nieh, J. Wadsworth, O.D. Sherby. *Superplasticity in Metals and Ceramics* (Cambridge University Press, Cambridge, UK, 1997)
[32] V.N. Perevezentsev, V.V. Rybin, V.N. Chuvil'deev. Acta Metall. Mater., **40**, 887 (1992). DOI: 10.1016/0956-7151(92)90065-M
[33] V.I. Feodos'ev. *Soprotivlenie materialov* (Nauka, M., 1967) (in Russian).
[34] A.G. Mochugovskiy, A.V. Mikhaylovskaya. Mater. Lett., **275**, 128096 (2020). DOI: 10.1016/j.matlet.2020.128096
[35] A.G. Mochugovskiy, A.V. Mikhaylovskaya, M.Yu. Zadorogny, I.S. Golovin. J. Alloys Compd., **856**, 157455 (2021). DOI: 10.1016/j.jallcom.2020.157455
[36] A.V. Mikhaylovskaya, A.G. Mochugovskiy, V.S. Levchenko, N.Yu. Tabachkova, W. Mifalo, V.K. Portnoy. Mater. Charact., **139**, 30 (2018). DOI: 10.1016/j.matchar.2018.02.030
[37] I.A. Zorin, E.V. Aryshenskii, A.M. Drits, S.V. Konovalov, V.S. Komarov. Izvestiya vuzov. Tsvetnaya metallurgiya, **1**, 56 (2023) (in Russian). DOI: 10.17073/0021-3438-2023-1-56-65
[38] I.A. Zorin, E.V. Aryshenskii, E.A. Kudryavtsev, A.M. Drits, S.V. Konovalov. Frontier Mater. Technol., **1**, 29 (2024) (in Russian). DOI: 10.18323/2782-4039-2024-1-67-3
[39] D.I. Sadykov, M.Yu. Murashkin, A.A. Kirilenko, A.A. Levin, A.I. Likhachev, T.S. Orlova. FTT, **66** (6), 933 (2024) (in Russian). DOI: 10.61011/FTT.2024.06.58250.119
[40] T.S. Orlova, T.A. Latynina, M.Yu. Murashkin, V.U. Kazykhanov. Phys. Solid State, **61** (12), 2509 (2019). DOI: 10.1134/S1063783419120357
[41] V.N. Perevezentsev, V.V. Rybin, V.N. Chuvil'deev. Acta Metall. Mater., **40**, 907 (1992). DOI: 10.1016/0956-7151(92)90067-O
[42] E.W. Hart. Acta Metall., **15**, 351 (1967). DOI: 10.1016/0001-6160(67)90211-8
[43] V.N. Chuvil'deev, O.E. Pirozhnikova, A.V. Nokhrin, M.M. Myshlyaev, Phys. Solid State, **49** (4), 684 (2007). DOI: 10.1134/S1063783407040142
[44] V.N. Chuvil'deev. *Neravnovesnye granitsy zeren v metallakh. Teoriya i prilozheniya* (Fizmatlit, M., 2004) (in Russian).
[45] V.N. Chuvil'deev, A.V. Nokhrin, O.E. Pirozhnikova, M.Yu. Gryaznov, Yu.G. Lopatin, M.M. Myshlyaev, V.I. Kopylov. Phys. Solid State, **59**, 1584 (2017). DOI: 10.1134/S1063783417080066
[46] V.N. Chuvil'deev, A.V. Shchavleva, A.V. Nokhrin, O.E. Pirozhnikova, M.Yu. Gryaznov, Yu.G. Lopatin, A.N. Sysoev, N.V. Melekhin, N.V. Sakharov, V.I. Kopylov, M.M. Myshlyaev. Phys. Solid State, **52** (5), 1098 (2010). DOI: 10.1134/S1063783410050422
[47] V.N. Perevezentsev, V.V. Rybin, V.N. Chuvil'deev. Acta Metall. Mater., **40**, 915 (1992). DOI: 10.1016/0956-7151(92)90068-P
[48] V.N. Perevezentsev, V.V. Rybin, V.N. Chuvil'deev. Poverkhnost': Fizika, khimiya, mekhanika, **11**, 130 (1986) (in Russian).
[49] V.N. Chuvil'deev, M.Y. Gryaznov, S.V. Shotin, V.I. Kopylov, A.V. Nokhrin, C.V. Likhnitskii, A.A. Murashov, A.A. Bobrov, N.Yu. Tabachkova, O.E. Pirozhnikova. J. Alloys Compd., **877**, 160099 (2021). DOI: 10.1016/j.jallcom.2021.160099
[50] M. Gryaznov, S. Shotin, A. Nokhrin, V. Chuvil'deev, C. Likhnitskii, V. Kopylov, M. Chegurov, N. Tabachkova, I. Shadrina, E. Smirnova, O. Pirozhnikova. Materials, **15**, 176 (2022). DOI: 10.3390/ma15010176
[51] B. Forbord, W. Lefebvre, F. Danoix, H. Hallem, K. Marthinsen. Scr. Mater., **51**, 333 (2004). DOI: 10.1016/j.scriptamat.2004.03.033
[52] C.B. Fuller, J.L. Murray, D.N. Seidman. Acta Mater., **53**, 5401 (2005). DOI: 10.1016/j.actamat.2005.08.016
[53] A.V. Nokhrin, M.Y. Gryaznov, S.V. Shotin, G.S. Nagicheva, M.K. Chegurov, A.A. Bobrov, V.I. Kopylov, V.N. Chuvil'deev. Metals, **13**, 133 (2023). DOI: 10.3390/met13010133
[54] I.S. Golovin, A.V. Mikhaylovskaya, H.-R. Sinning. J. Alloys Compd., **577**, 622 (2013). DOI: 10.1016/j.jallcom.2013.06.138

[55] A.V. Mikhaylovskaya, M.S. Kishchik, A.D. Kotov, N.Yu. Tabachkova. Mater. Lett., **321**, 132412 (2022). DOI: 10.1016/j.matlet.2022.132412
[56] T. Sakai, A. Belyakov, R. Kaibyshev, H. Miura, J.J. Jonas. Progr. Mater. Sci., **60**, 130 (2014). DOI: 10.1016/j.pmatsci.2013.09.002
[57] I.I. Novikov, V.K. Portnoy, A.O. Titov, D.Y. Belov. Scr. Mater., **42**, 899 (2000). DOI: 10.1016/S1359-6462(00)00310-9
[58] N.V. Melekhin. Problemy prochnosti i plastichnosti, **85**, 178 (2023) (in Russian). DOI: 10.32326/1814-9146-2023-85-2-178-188

Translated by M.Shevelev